Circadian timing-dependent myoblast differentiation and muscle regeneration

Nobuko Katoku-Kikyo[1,2], Ellen Paatela[1,2,#], Daniel L. Houtz[1], Britney Lee[1], Dane Munson[1,$], Xuerui Wang[1,4,5], Mohammed Hussein[1,4,5], Jasmeet Bhatia[1,4,5], Seunghyun Lim[1,3], Ce Yuan[1,3], Yoko Asakura[1,4,5], Atsushi Asakura[1,4,5,*], and Nobuaki Kikyo[1,2,6,*]

[1]Stem Cell Institute, [2]Department of Genetics, Cell Biology, and Development, [3]Bioinformatics and Computational Biology Graduate Program, [4]Paul & Sheila Wellstone Muscular Dystrophy Center, [5]Department of Neurology, University of Minnesota, Minneapolis, MN 55455, USA

[#]Present address: Molecular and Cellular Biology Graduate Program, University of Washington, Seattle, WA, 98195, USA

[$]Present address: Mayo Clinic Alix School of Medicine, Rochester, MN 55905, USA

[6]Lead Contact

[*]Correspondence: asakura@umn.edu and kikyo001@umn.edu.

ABSTRACT

Circadian rhythms regulate cell proliferation and differentiation but circadian control of tissue regeneration remains elusive at the molecular level. Here, we show that the circadian master regulators Per1 and Per2 are integral components defining the efficiency of myoblast differentiation and muscle regeneration. We found that the depletion of Per1 or Per2 suppressed myoblast differentiation *in vitro* and muscle regeneration *in vivo*, demonstrating their non-redundant functions. Both Per1 and Per2 directly activated Igf2, an autocrine promoter of myoblast differentiation, accompanied by Per-dependent recruitment of RNA polymerase II, dynamic histone modifications at the *Igf2* promoter and enhancer, and the promoter-enhancer interaction. This circadian epigenetic oscillation created a preferred time window for initiating myoblast differentiation. Consistently, muscle regeneration was faster if initiated at night when Per1, Per2, and Igf2 were highly expressed compared with morning. This study reveals the circadian timing as a significant factor for effective muscle cell differentiation and regeneration.

Regulation of mammalian circadian rhythms is centered around the Clock/Bmal1 complex, a ubiquitously expressed basic helix-loop-helix Per-Arnt-Single-minded (PAS) transcription factor dimer[1-4]. The complex binds the E-box (5'-CANNTG-3') in promoters and enhancers of thousands of genes to activates their transcription, including the *Cry* (*Cry1* and *Cry2*) and *Per* (*Per1-Per3*) genes. Gradually accumulated Cry and Per in turn bind Clock/Bmal1 on DNA and repress its transcription activity, forming a negative feedback loop. Subsequent phosphorylation and ubiquitination of Cry and Per lead to their degradation, allowing Clock/Bmal1 to resume activation of the target genes. This oscillating activity of Clock/Bmal1 creates transcriptional circadian rhythms in more than 20% of the genes in the genome in at least one tissue in the body. In addition, Clock/Bmal1 activates retinoic acid receptor-related orphan receptor proteins (RORα-RORγ) and reverse orientation c-erb proteins (Rev-erbα and Rev-erbβ), which compete for the retinoic acid-related orphan receptor response element (RORE) in the *Bmal1* promoter. Opposing activities of ROR as an activator and Rev-erb as a repressor of Clock/Bmal1 form the second circadian feedback loop. These feedback loops exist in every tissue examined (peripheral clocks), including skeletal muscle. In contrast, the central clock is located in the suprachiasmatic nucleus (SCN) in the hypothalamus, which is entrained by the light signal transmitted from the retina as the primary external cue (zeitgeber). The peripheral clock is entrained by various physiological factors such as body temperature, feeding time, and physical activity, in addition to the loose control by the central clock.

Circadian regulation is tightly integrated into the genetic program of muscle cell differentiation as demonstrated by several studies[5-7]. First, more than 2,000 genes, including the master myogenic regulators *MyoD* and *myogenin*, show circadian oscillation in abundance[5, 8-10]. Second, whereas Bmal1 promotes satellite cell proliferation and differentiation, and is required for muscle

regeneration[11, 12], Rev-erbα acts as an inhibitor of these processes[13]. Third, Clock/Bmal1 binds the E-box in the core enhancer of *MyoD* in a circadian manner; MyoD then binds the *Bmal1* enhancer and increases the amplitude of *Bmal1* expression, forming a feed-forward loop in myogenesis[14, 15]. Finally, we previously showed that Cry2 promotes myoblast proliferation and fusion during differentiation in a circadian manner through stabilization of mRNAs encoding cyclin D1, a G1/S phase transition driver, and Tmem176b, a transmembrane regulator for myogenic cell fusion[16].

Mouse Per1 and Per2 share 73.4 % sequence similarity at the amino acid level but are not functionally redundant. *Per1*$^{-/-}$ mice and *Per2*$^{-/-}$ mice are grossly normal and fertile; however, both knockout (KO) mice exhibit circadian periods up to 2 hr shorter than wild-type (WT) mice and eventually become arrhythmic in constant darkness[17-20]. In contrast, *Per1*$^{-/-}$*:Per2*$^{-/-}$ mice become arrhythmic immediately after transfer to constant darkness although they are morphologically normal and fertile. As for muscle phenotypes, *Per2*$^{-/-}$ mice show a 20% shorter running distance with a treadmill test compared with WT and *Per1*$^{-/-}$ mice although the length, weight, contractility, and abundance of several contractile proteins in the tibialis anterior (TA) muscle were similar in the three genotypes[21]. Unlike the extensively studied Bmal1's involvement, however, virtually nothing is known about whether and how *Per* genes contribute to myogenic differentiation and muscle regeneration.

The present study uncovered insulin-like growth factor 2 (Igf2) as a critical link between Per1/Per2 and myoblast differentiation. Igf2 is a necessary and well-characterized autocrine differentiation promoter of myoblasts that increases in secretion levels during differentiation[22-24]. Igf2 is also upregulated upon muscle injury and enhances regeneration[25-27]. Additionally, several single nucleotide polymorphisms of the human *IGF2* genes are associated with a loss of muscle strength following strenuous exercise[28, 29]. *Igf2* null mice display impaired growth at birth but

subsequently grow normally[30]. Igf2 binds the type I Igf1 receptor (Igf1r) with the highest affinity among several receptors, resulting in its auto-phosphorylation and subsequent activation of the PI3K/AKT pathway and the RAS/MAP kinase pathway[31, 32]. In particular, activation of p38α/β MAPK by phosphorylation is an essential downstream effector for the promotion of myoblast differentiation by Igf2[33, 34]. p38 achieves the pro-differentiation function by triggering cell cycle exit, activating myogenic transcription factors, and opening the chromatin of muscle gene promoters (see ref[35, 36] for references). Most Igf2 in blood and local tissues is bound by Igf-biding proteins (IGFBP1-IGFBP7), which up- or downregulate Igf2 functions[37]. For example, whereas IGFBP-3 inhibits myoblast differentiation[38], IGFBP-5 is induced during early myoblast differentiation and amplifies the auto-regulatory loop of Igf2 expression, resulting in promoted differentiation[39]. Starting from a phenotypic analysis of *Per* KO mice on myoblast differentiation and muscle regeneration, this study uncovered Per1/2-regulated circadian epigenetic preconditions of the *Igf2* gene in myoblast differentiation.

Results

Disrupted muscle regeneration and myoblast differentiation by Per depletion

To study the roles of Per1 and Per2 in skeletal muscle regeneration, TA muscle in *Per* KO mice was injured by barium chloride injection and their regeneration was assessed by a series of histological analyses. The mice were entrained at 12 hr-light [Zeitgeber Time (ZT) 0 - ZT12] and 12 hr-dark cycles (ZT12 - ZT24) for two weeks before experiments. TA muscle was damaged and harvested at ZT14; ZT14 (20:00) was selected to compare with the result of the antiphase time point (ZT2, 8:00) later. Hematoxylin eosin (HE) staining on day 4.5 post-injury demonstrated smaller myofibers with centrally-located nuclei, an indication of newly formed myofibers, in *Per1*$^{-/-}$, *Per2*$^{-/-}$, and particularly *Per1*$^{-/-}$*:Per2*$^{-/-}$ mice compared with WT mice (Fig. 1a-1c). This trend continued at least until day 14 and was also observed in uninjured myofibers, although the smallest size of *Per1*$^{-/-}$*:Per2*$^{-/-}$ myofibers became less obvious (Supplementary Fig. 1a,b). In addition, myofibers expressing embryonic myosin heavy chain (eMHC), a marker for newly generated myofibers, were smaller in *Per2*$^{-/-}$ and *Per1*$^{-/-}$*:Per2*$^{-/-}$ mice than those in WT and *Per1*$^{-/-}$ mice (Fig 1d,e). Furthermore, the kinetics of cell cycle exit of satellite cells in the KO mice were different from those in WT mice. During muscle regeneration, activated satellite cells re-enter the cell cycle [EdU (5-ethynyl-2'-deoxyuridine)(+)/MyoD(+) population], followed by exit from the cell cycle [EdU(-)/MyoD(+)] before terminal differentiation. Comparison of the frequency of each population on day 4.5 showed an increased frequency of EdU(+)/MyoD(+) cells in the single and double KO mice compared with WT mice (Fig. 1f,g). This finding could suggest delayed cell cycle exit of the satellite cells in the KO mice, which translates into delayed muscle regeneration on day 4.5. Finally, the single and double KO mice contained more scars on day 14 after injury as demonstrated by Sirius red stain, suggesting more extensive damage or delayed regeneration in

the KO mice (Fig. 1h,i). Uninjured *Per2*$^{-/-}$ and *Per1*$^{-/-}$*:Per2*$^{-/-}$ mice already contained more scars than WT mice although it was less severe than in day 14 mice, implying that natural turnover of myofibers was also disrupted in the KO mice. Together, these findings provide evidence that both Per1 and Per2 are necessary for the proper regeneration of TA muscle.

To understand cell-autonomous effects of *Per* KO, primary myoblasts (activated satellite cells) were purified from hind limb and induced to differentiate into myotubes with 5% horse serum *in vitro*. *Per1*$^{-/-}$, *Per2*$^{-/-}$, and *Per1*$^{-/-}$*:Per2*$^{-/-}$ myoblasts displayed delayed activation of MHC, a marker for differentiation, and increased frequency of EdU uptake compared with WT cells (Supplementary Fig. 1c-g). This result exhibited impaired differentiation of *Per* KO myoblasts, consistent with the delayed TA muscle regeneration.

To obtain a large number of cells for a mechanistic study, we examined whether the mouse myoblast cell line C2C12 could recapitulate the KO phenotypes of the primary myoblasts. The *Per1* or *Per2* gene was depleted by shRNA-mediated knockdown (KD) and CRISPR-Cas9-mediated KO (Supplementary Fig 2a,b). These cells were used in bulk without cloning because differentiation-resistant cells would have been selected by cloning. When the cells were induced to differentiate, MHC(+) cells were shorter and more sparse in the KD and KO cells than control cells on differentiation days 3 and 5 (Fig. 2a). This finding was quantified as decreased differentiation index (frequency of nuclei in MHC(+) cells among total nuclei) and fusion index (frequency of nuclei in MHC(+) cells containing more than one nuclei among total nuclei) in the KD and KO cells (Fig. 2b,c). The KO cells also demonstrated slightly delayed cell cycle exit during differentiation (Fig. 2d). Additionally, expression of differentiation-specific genes encoding myogenin (*Myog*), muscle creatinine kinase (*Ckm*), myomaker (*Mymk*), and MHC (*Myh3*) was decreased by the KD and KO (Fig. 2e). The similarity of the inhibited differentiation between *Per1*

KO and *Per2* KO cells was further highlighted by several transcriptome data sets. The list included a heat map, a principal component analysis, Venn diagrams of differentially expressed genes (more than 2,000 genes were commonly up- or downregulated more than 2-fold compared with control cells), scatter plots (R^2>0.97), and common representations of muscle-related pathways in a gene ontology analysis of the RNA-seq data on days 0, 3, and 5 (Fig. 2f,g and Supplementary Fig. 2c-f). These results indicate that both *Per1* and *Per2* are necessary for effective myoblast differentiation *in vitro*.

Downregulation of *Igf2* expression is a common consequence of *Per1* KO and *Per2* KO

The common phenotypes of *Per1* and *Per2* depletion led us to search for important myogenic genes that were commonly up- or downregulated by each KO. Analysis of the RNA-seq data revealed a substantial downregulation of *Igf2* by both *Per1* KO and *Per2* KO throughout differentiation from day 0 (undifferentiated) to day 5 (Supplementary Fig. 3a,b). This result was verified by qPCR of *Per* KD and KO cells (Fig. 3a). To investigate the involvement of Igf2 in the *Per* depletion phenotypes, *Igf2* was knocked down with two shRNAs in C2C12 cells (Supplementary Fig. 3c). MHC(+) cells in the KD cells were more sparse and shorter than control KD cells, consistent with the lower differentiation index and fusion index, as well as the decreased expression of differentiation-specific genes (Fig. 3b-e). Cell cycle exit was also delayed by *Igf2* KD during differentiation (Fig. 3f). Thus, *Igf2* depletion recapitulated the phenotypes of Per depletion.

Igf2 was likely to be expressed in a circadian manner as a downstream effector of Per1 and Per2. This possibility was tested by western blotting with C2C12 cells harvested every 4 hr after circadian synchronization with dexamethasone. The protein level of Bmal1 reached a peak at 44

hr after synchronization, which was anti-phasic to the expression patterns of Per1 and Per2 in control cells (Fig. 3g). Igf2 expression reached peaks at 32-36 hr and 56 hr, similar to the patterns of Per1 and Per2. Phosphorylation of p38 (p-p38) followed the expression pattern of Igf2 as its downstream effector. In contrast, Igf2 and p-p38 were severely downregulated in *Per* KO cells. *Igf2* was also expressed in TA muscle in a circadian manner but the rhythms were largely lost in *Per1*$^{-/-}$ and *Per2*$^{-/-}$ mice (Fig. 3h). These results verified that Igf2 expression is regulated by Per1 and Per2 in a circadian manner.

Next, the concentration of Igf2 in the culture supernatant of C2C12 cells was measured with ELISA. The concentration was approximately 0.025 ng/ml with undifferentiated cells and was increased 6-fold during differentiation as previously reported (Fig. 3i)[22]. Although Igf2 in the supernatant of *Per* KO cells was also increased, the level remained less than 20% of the control level on day 5, consistent with PCR and western blotting results. The Igf2 concentration with control cells also displayed oscillation that was similar to the western blotting result (Fig. 3j). The concentration represented the amount of accumulated Igf2 since 0 hr, when dexamethasone was replaced with fresh culture medium. The result likely reflected the gain by secretion and the loss by degradation and attachment to the culture dish and cell surface. The oscillation became more evident when an increase or a decrease between two time points were plotted (Fig. 3k).

We also examined whether exogenous Igf2 could rescue the disrupted differentiation of *Per* KO cells by adding Igf2 to the culture medium from day 0 onward. Igf2 raised differentiation index and fusion index 2- to 3-fold at >1 ng/ml but the indices did not reach the levels of the control cells (Supplementary Fig. 4a,b). In addition, the required concentrations were more than 10-times higher than that in the culture medium of the control cells. The high concentrations of Igf2 could also increase the *Myog* and *Ckm* mRNA close to the levels of the control cells that were not treated

with Igf2 (Supplementary Fig. 4c,d). Thus, Igf2 could partially rescue the disrupted differentiation of *Per* KO cells if an excessive amount was provided. Note that the concentration of effective Igf2 in the culture medium was unknown due to the presence of IGFBPs.

Epigenetic regulation of *Igf2* expression by Per1 and Per2

To elucidate how Per1 and Per2 promoted *Igf2* expression, epigenetic changes caused by *Per* KO were studied with ChIP-qPCR. An *Igf2* enhancer containing two E-boxes is embedded within an intron of the *Nctc1* gene located 105 kb downstream of the *Igf2* promoter[40, 41]. Publicly available ChIP-seq data obtained with non-synchronized myoblasts demonstrated binding peaks of Bmal1 and the histone acetylase p300 as well as the marker for enhancers H3K27ac (acetylation of lysine 27 in histone H3), but not another enhancer marker H3K4me1 (R3 region in Fig. 4a). Our ChIP-qPCR with synchronized control C2C12 cells detected binding peaks of Bmal1, Clock, Per1, and Per2 at similar time points and the patterns were preserved in *Per* KO cells (Fig. 4b,c and Supplementary Fig. 5a). However, the levels of H3K27ac, H3K4me1, and p300 were significantly decreased in *Per* KO cells, indicating Per1 and Per2 dependency of the histone modifications.

Muscle cells primarily utilize Promoter 3 among the three promoters of the *Igf2* gene[42, 43], which was verified by qPCR (Supplementary Fig. 6a,b). Downloaded ChIP-seq data with non-synchronized myoblasts did not show a specific increase or decrease of Bmal1, RNA polymerase II (Pol II), or histone markers for active genes (H3K4me3 and H3K9ac) and repressed genes (H3K27me3) at Promoter 3 (region R13 in Fig. 5a). However, synchronized C2C12 cells again demonstrated a Per-dependent increase (Pol II, H3K4me3, and H3K9ac) or decrease (H3K27me3) of these proteins at Promoters 3 and 1 (R15) (Fig. 5b,c and Supplementary Fig. 6c). Thus, both

Per1 and Per2 were necessary for the circadian dynamics of multiple epigenetic markers characteristic for gene activation at the *Igf2* enhancer and promoters.

To understand the functional significance of the circadian epigenetics, the temporal profile of nascent *Igf2* mRNA was quantified with synchronized cells. A nuclear run-on assay demonstrated that nascent *Igf2* mRNA was most abundant at time points when the *Igf2* enhancer and promoters were enriched with active gene markers in control cells (Fig. 6a, 36 hr and 60 hr). However, the *Igf2* level remained low throughout the process with *Per* KO cells as expected. Therefore, the circadian transcriptional changes of *Igf2* indeed reflected the epigenetic dynamics of the gene.

The interaction between the *Igf2* enhancer and Promoter 3 has been shown in differentiating myoblasts and skeletal muscle[41, 44]. Because chromatin interactions are also regulated by circadian rhythms[66, 67], we hypothesized that the *Igf2* enhancer-promoter interaction would also demonstrate circadian oscillation. This possibility was examined with Chromosome Conformation Capture (3C) by studying the interaction between Promoter 3 (anchor point in 3C) and the enhancer at 24 and 36 hr post-synchronization, which corresponded to the nadir and the peak of the *Igf2* level, respectively (Fig. 6b). The interaction (crosslinking frequency) at 36 hr was approximately twice as high as it was at 24 hr in control cells (Fig. 6c). This pattern was preserved in *Per* KO cells but the crosslinking efficiency became less than half compared with control cells (Fig. 6c,d). Thus, both Per1 and Per2 are required for the circadian dynamics of the promoter-enhancer interaction at the *Igf2* gene, just like the epigenetic modifications.

Coupling of differentiation efficiency and the circadian timing of differentiation initiation

The above findings led us to a hypothesis that myoblasts could differentiate more efficiently if differentiation cues are provided at the circadian timing when *Per1*, *Per2*, and *Igf2* are highly

expressed compared with other time points (precondition). This was evaluated with C2C12 cells that were induced to differentiate at different time points after synchronization. Indeed, the cells differentiated more efficiently when induced at 36 hr and 60 hr post-synchronization compared with 24 hr and 48 hr as demonstrated by higher differentiation index, fusion index, and the expression levels of differentiation-specific genes (*Myh3*, *Myog*, and *Ckm*) and *Igf2* after 48 hr of differentiation (Fig. 6e-i). This trend was in agreement with the epigenetic modifications of the *Igf2* promoters and enhancer. Note that since the cells kept proliferation between 24 hr and 60 hr before the differentiation induction, the increased cell density *per se* could promote differentiation in the later phase. In this sense, the drop of the differentiation efficiency at 44 - 48 hr in comparison to 36 hr was more significant than the increased differentiation from 48 hr to 60 hr. *Igf2* KD cells differentiated poorly regardless of when differentiation was initiated (Supplementary Fig. 7a-c).

Since *Per1*, *Per2*, and *Igf2* were also expressed in TA muscle in a circadian manner, the timing of injury could be an important factor for muscle regeneration. To assess this possibility, TA muscle was injured at ZT2 (low *Per1*, *Per2*, and *Igf2*; the early inactive phase of mice) and ZT14 (high *Per1*, *Per2*, and *Igf2*; the early active phase) to compare the regeneration efficiency. HE staining clearly showed larger TA muscle in the ZT14 WT mice than in the ZT2 mice on day 4.5 and this difference was lost by day 14 (Fig. 7a,b and Supplementary Fig. 7d). There was no statistically significant difference between ZT2 and ZT14 injuries in the single and double KO mice of *Per*1 and *Per2*. The average diameter of eMHC(+) myofibers was also longer in WT mice damaged at ZT14 than that in the ZT2 damage and this difference was also lost in the single and double KO mice (Fig. 7c,d). Moreover, the frequency of the EdU(+)/MyoD(+) population was diminished in the ZT14 WT mice compared with ZT2 mice on day 4.5 and 5.5, suggesting early cell cycle exit (Fig. 7e,f). Finally, scar formation was also less abundant in the ZT14 WT mice than in the ZT2

mice on day 14; this difference was again erased in the single and double KO mice (Fig. 7. g,h). These results collectively indicate that circadian timing of injury affects the efficiency of TA muscle regeneration in a *Per1*- and *Per2*-dependent manner.

DISCUSSION

The central message of the present work is that the efficiency of myoblast differentiation and muscle regeneration is dependent on the circadian timing when these events are triggered. As a mechanistic explanation obtained with the myoblast model, the *Igf2* gene was preconditioned toward activation in a circadian manner while the cells were still in the proliferation medium. Despite extensive studies of circadian regulation of cell proliferation and differentiation[45, 46], studies focused on the mechanistic influence of circadian timing on tissue regeneration are quite limited. One of the few studies concerns fibroblast migration during skin wound healing[47]. Fibroblast mobilization to a mouse skin incision site, an early and essential step in wound healing, was greater when the wound was inflicted at ZT13 than at ZT5. Additionally, when a skin explant was harvested at different time points and immediately wounded by a biopsy punch, the number and volume of fibroblasts invading the wound area were higher in the explant harvested at ZT13 than at ZT5. Circadian regulation of actin polymerization, which controls migration and adhesion, is one of the mechanisms for the time-dependent difference in the wound healing efficiency. In a related phenomenon, circadian timing of physical exercise influences muscle strength and oxidative capacity[48]. For example, muscle atrophy in the mouse hind limb due to reduced gravity was prevented more effectively by intermittent weigh bearing at ZT12-ZT16 than at ZT20-ZT0[49]. Based on our results, circadian timing could affect the recovery from muscle damage caused by trauma and surgery.

Our findings on the circadian timing-dependent differentiation and regeneration should be interpreted in a broader perspective of circadian metabolic regulation that defines the availability of energy and cellular building blocks[50-52]. A circadian transcriptome analysis of muscle uncovered clustered expression of genes with a common metabolic function at specific circadian phases in

the mouse under constant darkness with *ad libitum* feeding[53]. Specifically, the genes involved in carbohydrate catabolism (the early active/dark phase), carbohydrate storage (the mid-active/dark), lipogenesis (the end of the active/dark phase), and fatty-acid uptake and β-oxidation (the mid-inactive/light phase) reached peaks at distinct circadian phases as indicated in the parentheses. Metabolomic profiling of muscle also demonstrated neutral lipid storage and decreased lipid and protein catabolism in the late inactive phase[54]. Given the global circadian oscillation of the numerous metabolites essential for tissue turnover, circadian timing could create a preferred time window for an effective response to major tissue disruption and repair although experimental evidence is lacking. The interaction between the Per/Igf2 axis and the global metabolic oscillation awaits further studies.

The notion of the preferred time window also needs to be assessed in relation to other muscle regulators that exhibit circadian expression patterns. For example, glucocorticoids are major circadian modulators of multiple activities, including energy metabolism and tissue regeneration. The glucocorticoid secretion is characterized by robust circadian oscillation with a daily peak at the start of the activity (early night for mouse)[55, 56]. Glucocorticoids promote myofiber repair after injury via increased expression of the immunomodulators annexins A1 and A6, both of which are also involved in muscular dystrophy phenotypes[57, 58]. It remains to be elucidated how glucocorticoids, along with other muscle regulators Bmal1, Rev-erbα, and Cry2 mentioned earlier, interact with the Per/Igf2 axis in organizing circadian timing-dependent muscle cell differentiation and regeneration.

Various histone modifications oscillate at circadian-regulated genes through the recruitment of responsible enzymes as binding partners of the Clock/Bmal1 complex[4, 59]. The modifications include markers for gene activation, such as acetylation by p300 and CREB-Binding Protein (CBP)

as well as H3K4me3 by mixed lineage leukemia 1 (MLL1), and those for gene repression, including deacetylation by Sirtuin-1 (SIRT1) and H3K27me3 by Enhancer of Zeste 2 (EZH2). Reflecting the roles of the Per proteins as negative regulators, their binding partners include well-known chromatin repressive complexes, such as HP1γ-Suv39h (induces H3K9me2 and H3K9me3) and deacetylase complexes Sin3 and NuRD. The vast majority of these studies used mouse liver and embryonic fibroblasts as model materials, leaving tissue-specific variability under-explored. In our study, more than 1,000 genes were commonly activated by *Per 1* KO and *Per2* KO cells, suggesting that Per1 and Per2 can act as gene activators in a context-dependent manner. Per-induced activation has been demonstrated with several genes involved in sodium channels in the kidney[60-62]. Whereas Per1 directly inhibits the expression of the *WNK4* gene, it activates the *NCC* and *WNK1* genes in a mouse renal tubular cell line[60]. In another example, Bmal1 and Per1 are required for the circadian activation of prolactin in a rat mammotrope cell line[63]. Moreover, Per2 activates *Cry1* by removing the Clock/Bmal1/Cry1 repressor complex from the *Cry1* promoter in an ectopic expression model[64]. This study also showed that genes with complex promoters can be repressed or de-repressed by Per, depending on the regulatory elements at the promoters. Identification of the binding proteins of Per1 and Per2 would be an important next step to further clarify how Per1 and Per2 activate *Igf2* during myoblast differentiation.

Long-range interactions between enhancers and promoters are achieved by chromatin loop formation, which is mediated by CCCTC-binding factor (CTCF) and the cohesin complex at the anchors of the loops and YY1 at the interface between promoters and enhancers[65]. Chromatin loop formation is one of the emerging mechanisms underlying oscillating gene activity[66, 67]. For example, the *Cry1* gene promoter interacts with its enhancer in the first intron in a synchronized manner with oscillating gene expression in the liver[68]. Little is known, however, about the direct

interface between the circadian master proteins and the loop proteins. One of few examples is Rev-Erbα, which prevents the loop formation by recruiting the NCoR-HDAC3 repressive complex and removing the Mediator complex, a promoter of enhancer-promoter interactions[69]. Unidentified binding proteins of Per proteins are undoubtedly involved in the loop formation at the *Igf2* gene.

This study revealed circadian regulation of myoblast differentiation and muscle regeneration and demonstrated epigenetic regulation of the *Igf2* gene by Per1 and Per2 as one of the underlying mechanisms using a myoblast differentiation model. Future genome-wide epigenetic analysis of histone modifications and chromatin interactions would further uncover other unexpected underpinnings for the time-of-the-day-dependent regeneration of muscle and other tissues.

Author contribution

A.A. and N.K. conceived experiments and analyzed data. N,K-K., E.P, D.L.H., B.L., D.M., X.W., M.H., J.B., Y.A., A.A., and N.K. performed experiments. S.L. and C.Y. analyzed bioinformatics data. A.A. and N.K. wrote the manuscript. All edited the manuscript.

Acknowledgements

We thank James Staats, Brian Ruis, and Allison Keith for technical supports and Karyn A Esser for critical reading of the manuscript. We acknowledge Minnesota Supercomputing Institute, University of Minnesota Informatics Institute, and University of Minnesota Genomics Center for providing high-performance computing resources and the gopher-pipelines. S.L. and C.Y. were supported by the Minnesota Stem Cell Institute. A.A. was supported by the NIH (R01 AR062142 and R21 AR070319). N.K was supported by the NIH (R01 GM137603 and R21 AR076167), Regenerative Medicine Minnesota (RMM 101617 DS 004), and Grant-in-Aid of Research University of Minnesota (291987). The content is solely the responsibility of the authors and does not necessarily represent the official views of the NIH.

Competing interests

The authors declare no competing interests.

REFERENCES

1. Hirano, A., Fu, Y.H. & Ptacek, L.J. The intricate dance of post-translational modifications in the rhythm of life. *Nat Struct Mol Biol* **23**, 1053-1060 (2016).
2. Takahashi, J.S. Transcriptional architecture of the mammalian circadian clock. *Nat Rev Genet* **18**, 164-179 (2017).
3. Gustafson, C.L. & Partch, C.L. Emerging models for the molecular basis of mammalian circadian timing. *Biochemistry* **54**, 134-149 (2015).
4. Papazyan, R., Zhang, Y. & Lazar, M.A. Genetic and epigenomic mechanisms of mammalian circadian transcription. *Nat Struct Mol Biol* **23**, 1045-1052 (2016).
5. Harfmann, B.D., Schroder, E.A. & Esser, K.A. Circadian rhythms, the molecular clock, and skeletal muscle. *J Biol Rhythms* **30**, 84-94 (2015).
6. Lefta, M., Wolff, G. & Esser, K.A. Circadian rhythms, the molecular clock, and skeletal muscle. *Curr Top Dev Biol* **96**, 231-271 (2011).
7. Mayeuf-Louchart, A., Staels, B. & Duez, H. Skeletal muscle functions around the clock. *Diabetes Obes Metab* **17 Suppl 1**, 39-46 (2015).
8. Pizarro, A., Hayer, K., Lahens, N.F. & Hogenesch, J.B. CircaDB: a database of mammalian circadian gene expression profiles. *Nucleic Acids Res* **41**, D1009-1013 (2013).
9. McCarthy, J.J. *et al.* Identification of the circadian transcriptome in adult mouse skeletal muscle. *Physiol Genomics* **31**, 86-95 (2007).
10. Miller, B.H. *et al.* Circadian and CLOCK-controlled regulation of the mouse transcriptome and cell proliferation. *Proc Natl Acad Sci U S A* **104**, 3342-3347 (2007).
11. Chatterjee, S. *et al.* Brain and muscle Arnt-like 1 is a key regulator of myogenesis. *J Cell Sci* **126**, 2213-2224 (2013).

12. Chatterjee, S., Yin, H., Nam, D., Li, Y. & Ma, K. Brain and muscle Arnt-like 1 promotes skeletal muscle regeneration through satellite cell expansion. *Exp Cell Res* **331**, 200-210 (2015).

13. Chatterjee, S. *et al.* The Nuclear Receptor and Clock Repressor Rev-erbalpha Suppresses Myogenesis. *Sci Rep* **9**, 4585 (2019).

14. Andrews, J.L. *et al.* CLOCK and BMAL1 regulate MyoD and are necessary for maintenance of skeletal muscle phenotype and function. *Proc Natl Acad Sci U S A* **107**, 19090-19095 (2010).

15. Hodge, B.A. *et al.* MYOD1 functions as a clock amplifier as well as a critical co-factor for downstream circadian gene expression in muscle. *Elife* **8** (2019).

16. Lowe, M. *et al.* Cry2 is critical for circadian regulation of myogenic differentiation by Bclaf1-mediated mRNA stabilization of cyclin D1 and Tmem176b. *Cell Rep* **22**, 2118-2132, (2018).

17. Cermakian, N., Monaco, L., Pando, M.P., Dierich, A. & Sassone-Corsi, P. Altered behavioral rhythms and clock gene expression in mice with a targeted mutation in the Period1 gene. *EMBO J* **20**, 3967-3974 (2001).

18. Bae, K. *et al.* Differential functions of mPer1, mPer2, and mPer3 in the SCN circadian clock. *Neuron* **30**, 525-536 (2001).

19. Zheng, B. *et al.* The mPer2 gene encodes a functional component of the mammalian circadian clock. *Nature* **400**, 169-173 (1999).

20. Zheng, B. *et al.* Nonredundant roles of the mPer1 and mPer2 genes in the mammalian circadian clock. *Cell* **105**, 683-694 (2001).

21. Bae, K. *et al.* Differential effects of two period genes on the physiology and proteomic profiles of mouse anterior tibialis muscles. *Mol Cells* **22**, 275-284 (2006).

22. Florini, J.R. *et al.* "Spontaneous" differentiation of skeletal myoblasts is dependent upon autocrine secretion of insulin-like growth factor-II. *J Biol Chem* **266**, 15917-15923 (1991).

23. Yoshiko, Y., Hirao, K. & Maeda, N. Differentiation in C(2)C(12) myoblasts depends on the expression of endogenous IGFs and not serum depletion. *Am J Physiol Cell Physiol* **283**, C1278-1286 (2002).

24. Duan, C., Ren, H. & Gao, S. Insulin-like growth factors (IGFs), IGF receptors, and IGF-binding proteins: roles in skeletal muscle growth and differentiation. *Gen Comp Endocrinol* **167**, 344-351 (2010).

25. Keller, H.L., St Pierre Schneider, B., Eppihimer, L.A. & Cannon, J.G. Association of IGF-I and IGF-II with myofiber regeneration in vivo. *Muscle Nerve* **22**, 347-354 (1999).

26. Levinovitz, A., Jennische, E., Oldfors, A., Edwall, D. & Norstedt, G. Activation of insulin-like growth factor II expression during skeletal muscle regeneration in the rat: correlation with myotube formation. *Mol Endocrinol* **6**, 1227-1234 (1992).

27. Kirk, S.P., Oldham, J.M., Jeanplong, F. & Bass, J.J. Insulin-like growth factor-II delays early but enhances late regeneration of skeletal muscle. *J Histochem Cytochem* **51**, 1611-1620 (2003).

28. Baumert, P., Lake, M.J., Stewart, C.E., Drust, B. & Erskine, R.M. Genetic variation and exercise-induced muscle damage: implications for athletic performance, injury and ageing. *Eur J Appl Physiol* **116**, 1595-1625 (2016).

29. Devaney, J.M. *et al.* IGF-II gene region polymorphisms related to exertional muscle damage. *J Appl Physiol (1985)* **102**, 1815-1823 (2007).

30. Baker, J., Liu, J.P., Robertson, E.J. & Efstratiadis, A. Role of insulin-like growth factors in embryonic and postnatal growth. *Cell* **75**, 73-82 (1993).

31. Siddle, K. Signalling by insulin and IGF receptors: supporting acts and new players. *J Mol Endocrinol* **47**, R1-10 (2011).

32. Taniguchi, C.M., Emanuelli, B. & Kahn, C.R. Critical nodes in signalling pathways: insights into insulin action. *Nat Rev Mol Cell Biol* **7**, 85-96 (2006).

33. Knight, J.D. & Kothary, R. The myogenic kinome: protein kinases critical to mammalian skeletal myogenesis. *Skelet Muscle* **1**, 29 (2011).

34. Segales, J., Perdiguero, E. & Munoz-Canoves, P. Regulation of Muscle Stem Cell Functions: A Focus on the p38 MAPK Signaling Pathway. *Front Cell Dev Biol* **4**, 91 (2016).

35. Gardner, S., Gross, S.M., David, L.L., Klimek, J.E. & Rotwein, P. Separating myoblast differentiation from muscle cell fusion using IGF-I and the p38 MAP kinase inhibitor SB202190. *Am J Physiol Cell Physiol* **309**, C491-500 (2015).

36. Segales, J. *et al.* Chromatin-wide and transcriptome profiling integration uncovers p38alpha MAPK as a global regulator of skeletal muscle differentiation. *Skelet Muscle* **6**, 9 (2016).

37. Allard, J.B. & Duan, C. IGF-Binding Proteins: Why Do They Exist and Why Are There So Many? *Front Endocrinol (Lausanne)* **9**, 117 (2018).

38. Huang, X.Y. *et al.* Pancreatic cancer cell-derived IGFBP-3 contributes to muscle wasting. *J Exp Clin Cancer Res* **35**, 46 (2016).

39. Ren, H., Yin, P. & Duan, C. IGFBP-5 regulates muscle cell differentiation by binding to IGF-II and switching on the IGF-II auto-regulation loop. *J Cell Biol* **182**, 979-991 (2008).

40. Alzhanov, D. & Rotwein, P. Characterizing a distal muscle enhancer in the mouse Igf2 locus. *Physiol Genomics* **48**, 167-172 (2016).

41. Alzhanov, D.T., McInerney, S.F. & Rotwein, P. Long range interactions regulate Igf2 gene

transcription during skeletal muscle differentiation. *J Biol Chem* **285**, 38969-38977 (2010).

42. Kou, K. & Rotwein, P. Transcriptional activation of the insulin-like growth factor-II gene during myoblast differentiation. *Mol Endocrinol* **7**, 291-302 (1993).

43. Baral, K. & Rotwein, P. The insulin-like growth factor 2 gene in mammals: Organizational complexity within a conserved locus. *PLoS One* **14**, e0219155 (2019).

44. Yoon, Y.S. *et al.* Analysis of the H19ICR insulator. *Mol Cell Biol* **27**, 3499-3510 (2007).

45. Paatela, E., Munson, D. & Kikyo, N. Circadian Regulation in Tissue Regeneration. *Int J Mol Sci* **20** (2019).

46. Dierickx, P., Van Laake, L.W. & Geijsen, N. Circadian clocks: from stem cells to tissue homeostasis and regeneration. *EMBO reports* **19**, 18-28 (2018).

47. Hoyle, N.P. *et al.* Circadian actin dynamics drive rhythmic fibroblast mobilization during wound healing. *Science Translational Medicine* **9**, eaal2774-eaal2774 (2017).

48. Wolff, C.A. & Esser, K.A. Exercise Timing and Circadian Rhythms. *Curr Opin Physiol* **10**, 64-69 (2019).

49. Aoyama, S. *et al.* Day-Night Oscillation of Atrogin1 and Timing-Dependent Preventive Effect of Weight-Bearing on Muscle Atrophy. *EBioMedicine* **37**, 499-508 (2018).

50. Panda, S. Circadian physiology of metabolism. *Science* **354**, 1008-1015 (2016).

51. Aoyama, S. & Shibata, S. Time-of-Day-Dependent Physiological Responses to Meal and Exercise. *Front Nutr* **7**, 18 (2020).

52. Aoyama, S. & Shibata, S. The Role of Circadian Rhythms in Muscular and Osseous Physiology and Their Regulation by Nutrition and Exercise. *Front Neurosci* **11**, 63 (2017).

53. Hodge, B.A. *et al.* The endogenous molecular clock orchestrates the temporal separation of substrate metabolism in skeletal muscle. *Skelet Muscle* **5**, 17 (2015).

54. Dyar, K.A. *et al.* Transcriptional programming of lipid and amino acid metabolism by the skeletal muscle circadian clock. *PLoS Biol* **16**, e2005886 (2018).

55. Oster, H. *et al.* The Functional and Clinical Significance of the 24-Hour Rhythm of Circulating Glucocorticoids. *Endocr Rev* **38**, 3-45 (2017).

56. Dickmeis, T. Glucocorticoids and the circadian clock. *J Endocrinol* **200**, 3-22 (2009).

57. Shimizu-Motohashi, Y. *et al.* Pregnancy-induced amelioration of muscular dystrophy phenotype in mdx mice via muscle membrane stabilization effect of glucocorticoid. *PLoS One* **10**, e0120325 (2015).

58. Quattrocelli, M. *et al.* Intermittent glucocorticoid steroid dosing enhances muscle repair without eliciting muscle atrophy. *J Clin Invest* **127**, 2418-2432 (2017).

59. Takahashi, J.S. Transcriptional architecture of the mammalian circadian clock. *Nature reviews. Genetics* **18**, 164-179 (2017).

60. Richards, J. *et al.* A role for the circadian clock protein Per1 in the regulation of the NaCl co-transporter (NCC) and the with-no-lysine kinase (WNK) cascade in mouse distal convoluted tubule cells. *J Biol Chem* **289**, 11791-11806 (2014).

61. Gumz, M.L. *et al.* The circadian clock protein Period 1 regulates expression of the renal epithelial sodium channel in mice. *J Clin Invest* **119**, 2423-2434 (2009).

62. Stow, L.R. *et al.* The circadian protein period 1 contributes to blood pressure control and coordinately regulates renal sodium transport genes. *Hypertension* **59**, 1151-1156 (2012).

63. Bose, S. & Boockfor, F.R. Episodes of prolactin gene expression in GH3 cells are dependent on selective promoter binding of multiple circadian elements. *Endocrinology* **151**, 2287-2296 (2010).

64. Chiou, Y.Y. *et al.* Mammalian Period represses and de-represses transcription by displacing

CLOCK-BMAL1 from promoters in a Cryptochrome-dependent manner. *Proc Natl Acad Sci U S A* **113**, E6072-E6079 (2016).

65. Schoenfelder, S. & Fraser, P. Long-range enhancer-promoter contacts in gene expression control. *Nat Rev Genet* **20**, 437-455 (2019).

66. Pacheco-Bernal, I., Becerril-Perez, F. & Aguilar-Arnal, L. Circadian rhythms in the three-dimensional genome: implications of chromatin interactions for cyclic transcription. *Clin Epigenetics* **11**, 79 (2019).

67. Yeung, J. *et al.* Transcription factor activity rhythms and tissue-specific chromatin interactions explain circadian gene expression across organs. *Genome Res* **28**, 182-191 (2018).

68. Mermet, J. *et al.* Clock-dependent chromatin topology modulates circadian transcription and behavior. *Genes Dev* **32**, 347-358 (2018).

69. Kim, Y.H. *et al.* Rev-erbalpha dynamically modulates chromatin looping to control circadian gene transcription. *Science* **359**, 1274-1277 (2018).

Figure Legends

Fig. 1. Regeneration of TA muscle in *Per1*$^{-/-}$, *Per2*$^{-/-}$, and *Per1*$^{-/-}$:*Per2*$^{-/-}$ mice

a, HE staining of day 4.5 TA muscle sections. TA muscle was injured with barium chloride at ZT14 on day 0 and EdU was intraperitoneally injected 96 hr later for **f** and **g**. The muscle was harvested 12 hr later as day 4.5. Bar, 100 μm.

b, Size distribution of HE-stained myofibers containing centrally-located nuclei on day 4.5. The minimal Feret's diameter in each myofiber was measured. n = 8 mice in each group, including 4 males and 4 females, in **b** and **c**.

c, Average of the minimal Feret's diameters of myofibers with centrally-located nuclei on day 4.5.

d, Immunofluorescence staining of TA muscle with antibodies against eMHC and laminin (shows the border of each myofiber) on day 4.5. DNA was counterstained with DAPI. Bar, 100 μm.

e, Average of the minimal Feret's diameters of eMHC(+) areas on day 4.5. n = 4 mice.

f, Immunofluorescence staining of TA muscle sections with the MyoD antibody and the EdU kit. Mice were injected with EdU on day 4 post-injury and TA muscle was harvested on day 4.5 for the staining. Bar, 25 μm.

g, Frequency of positive cells for EdU uptake and MyoD staining shown in **f**. n = 4 mice.

h, Sirius red staining of days 7 and 14 post-injury and uninjured TA muscle. Bar, 200 μm.

i, The area percentage of Sirius red(+) fibrosis indicated in **h**.

Data are presented as mean + SEM in **c**, **e**, **g**, and **i**. * $p < 0.05$, ** $p < 0.01$, and *** $p<0.001$ with Student's t-test in comparison to WT.

Fig. 2. Differentiation of C2C12 cells after depletion of *Per1* and *Per2*

a, Immunofluorescence staining of C2C12 cells with MHC antibody during differentiation with

5% horse serum. *Per1* and *Per2* were depleted with shRNA (KD) and CRISPR-Cas9 (KO). Non-targeting sequences were used as each control. Bar, 100 μm.

b, Differentiation index on days 3 and 5.

c, Fusion index on days 3 and 5.

d, Temporal profile of the frequency of EdU(+) nuclei in KO cells during differentiation.

e, Relative expression levels of five muscle genes determined by qPCR during differentiation. The value obtained with control cells on day 0 (before differentiation) was defined as 1.0 for each gene.

f, Heat map comparing the transcriptome of KO cells.

g, Principal component analysis of KO cells.

Data are presented as mean + or ± SEM of n=3 biological replicates in **b**, **c**, **d**, and **e**. * $p < 0.05$, ** $p < 0.01$, and *** $p<0.001$ with Student's t-test in comparison to control.

Fig. 3. The expression pattern and depletion of Igf2 in C2C12 cells

a, Relative expression levels of *Igf2* determined by qPCR during differentiation of C2C12 cells after depletion of *Per1* and *Per2*. The value obtained with control KD on day 0 (before differentiation) was defined as 1.0.

b, MHC staining of differentiating C2C12 cells after *Igf2* KD with two shRNAs. Bar, 200 μm.

c, Differentiation index during differentiation.

d, Fusion index during differentiation.

e, Relative expression levels of five muscle genes determined by qPCR during differentiation. The value obtained with day 0 control KD cells was defined as 1.0.

f, Temporal profile of the frequency of EdU(+) nuclei in *Per* KO cells during differentiation.

g, Western blotting with control and *Per* KO cells harvested every 4 hr after synchronization of the circadian rhythms. Histone H2B was used as a loading control.

h, Relative expression levels of *Per1*, *Per2*, and *Igf2* in TA muscle measured by qRT-PCR. The value of a WT mouse at ZT2 was defined as 1.0. n=3 mice with technical triplicates each.

i, Igf2 concentration in the supernatant of C2C12 cells during differentiation measured with ELISA. Culture medium was not replaced for 48 hr before measurement.

j, Igf2 concentration in the supernatant of C2C12 cells after circadian synchronization. Cells were treated with dexamethasone between -1 and 0 hr for synchronization. The culture medium was replaced with fresh growth medium at 0 hr and was not changed until harvest at the indicated time point. The concentration indicates the accumulated Igf2 in the medium.

k, The change of the Igf2 concentration in **j** was highlighted by displaying the change of the concentration between two time points.

Data are presented as mean + or ± SEM of n=3 biological replicates in **a**, **c-f**, and **h-k**. * $p < 0.05$, ** $p < 0.01$, and *** $p<0.001$ with Student's t-test compared with control cells.

Fig. 4. ChIP analyses of the *Igf2* enhancer

a, ChIP-seq analyses of the *Igf2* enhancer within the *Nctc1* gene downloaded from the Gene Expression Omnibus (GEO) database. See online methods for the accession number of each data set. R1 - R5 indicate the regions amplified by PCR in **b** and **c**.

b, ChIP-PCR analyses of indicated proteins in control and *Per* KO C2C12 cells. Relative abundance compared with input is shown.

c, Data in the R3 region in **b** are selectively shown as mean ± SEM. The peaks of control cells that are higher than those of *Per1* KO and *Per2* KO cells are highlighted with ** ($p < 0.01$ with

Student's t-test) and *** ($p < 0.001$). n=3 biological replicates in **b** and **c**.

Fig. 5. ChIP analyses of the *Igf2* promoters

a, ChIP-seq analyses of the *Igf2* promoters downloaded from the Gene Expression Omnibus (GEO) database. See online methods for the accession number of each data set. R11 - R17 indicate the regions amplified by PCR in **b** and **c**.

b, ChIP-PCR analyses of indicated proteins in control and *Per* KO C2C12 cells. Relative abundance compared with input is shown.

c, Data in the region R13 in **b** are selectively shown as mean ± SEM. The peaks (or nadirs) of control cells that are higher (or lower) than those of *Per1* KO and *Per2* KO cells are highlighted with ** ($p < 0.01$ with Student's t-test) and *** ($p < 0.001$). n=3 biological replicates in **b** and **c**.

Fig. 6. Circadian regulation of the *Igf2* gene and C2C12 cell differentiation

a, Nascent transcript analysis with a nuclear run-on assay comparing control and *Per* KO cells. Synchronized C2C12 cells were labeled with 5-ethynyl uridine (EU) for 4 hr before harvesting every 4 hr and EU(+) RNA was isolated with a kit, followed by RT-PCR of the indicated genes.

b, Locations of the primers used in the 3C experiments and BamHI sites in relation to the *Igf2* Promoter 3 and enhancer within the *Nctc1* genes. The primer shown in red was used in combination with one of the primers shown in black in 3C and the results were plotted in **c**.

c and **d**, Relative crosslinking frequency obtained with 3C comparing different time points (**c**) and *Per* KO cells and control (**d**). The value obtained with the *Clock* gene primers was defined as 1.0.

e, Schedule of circadian synchronization and initiation of differentiation. After incubation with

dexamethasone between -1 hr and 0 hr, the culture medium was replaced with growth medium containing 10% fetal bovine serum at 0 hr. The culture medium was replaced with differentiation medium (DM) containing 5% horse serum at different time points every 4 hr (arrows). Differentiation was continued for 48 hr from each starting point before fixation or harvest for various analyses.

f, Immunofluorescence staining C2C12 cells 48 hr after starting differentiation at indicated time points shown in **e**. Bar, 200 μm.

g-i, Analyses of differentiation index (**g**), fusion index (**h**), and relative expression of differentiation-specific genes (**i**) with C2C12 cells that were induced to differentiate at the indicated post-synchronization time points.

* $p < 0.05$, ** $p < 0.01$, and *** $p<0.001$ with Student's t-test comparing two time points (**c** and **g-i**) and control and *Per* KO cells (**d**). Graphs show mean ± SEM of n=3 biological replicates in **a**, **c**, **d**, and **g-i**.

Fig. 7. Differential regeneration efficiency of TA muscle depending on the circadian timing of the injury

a, Size distribution of HE-stained myofibers containing centrally-located nuclei on day 4.5. TA muscle was injured with barium chloride at ZT2 or ZT14 on day 0 and EdU was intraperitoneally injected 96 hr later for **e** and **f**. The muscle was harvested 12 hr later as day 4.5. The minimal Feret's diameter of each myofiber was calculated. n = 8 mice with 4 males and 4 females in each group in **a** and **b**.

b, Average of the minimal Feret's diameters of myofibers with centrally-located nuclei on day 4.5. 2 and 14 at the end of each genotype indicate the injury time at ZT2 and ZT14, respectively.

c, Immunofluorescence staining of WT TA muscle injured at ZT2 and ZT14 with antibodies against eMHC and laminin on day 4.5. DNA was counterstained with DAPI. Bar, 100 μm.

d, Average of the minimal Feret's diameters of the eMHC(+) areas on day 4.5. n = 4 mice.

e. Immunofluorescence staining of WT TA muscle sections with the MyoD antibody and the EdU kit. TA muscle was injured with barium chloride at ZT2 or ZT14 on day 0 and EdU was intraperitoneally injected 96 or 120 hr later. The muscle was harvested 12 hr later as day 4.5 or 5.5. Bar, 25 μm.

f, Frequency of positive cells for EdU uptake and MyoD staining in TA muscle sections shown in **e**. n = 4 mice.

g, Sirius red staining of WT TA muscle on day 14 post-injury. Bar, 200 μm.

h, The area percentage of fibrosis indicated by positive Sirius red staining on days 7 and 14.

Data are presented as mean + SEM in **b**, **d**, **f**, and **h**. * $p < 0.05$, ** $p < 0.01$, and *** $p<0.001$ with Student's t-test. The values at ZT14 in Fig. 1 were reused in these figures.

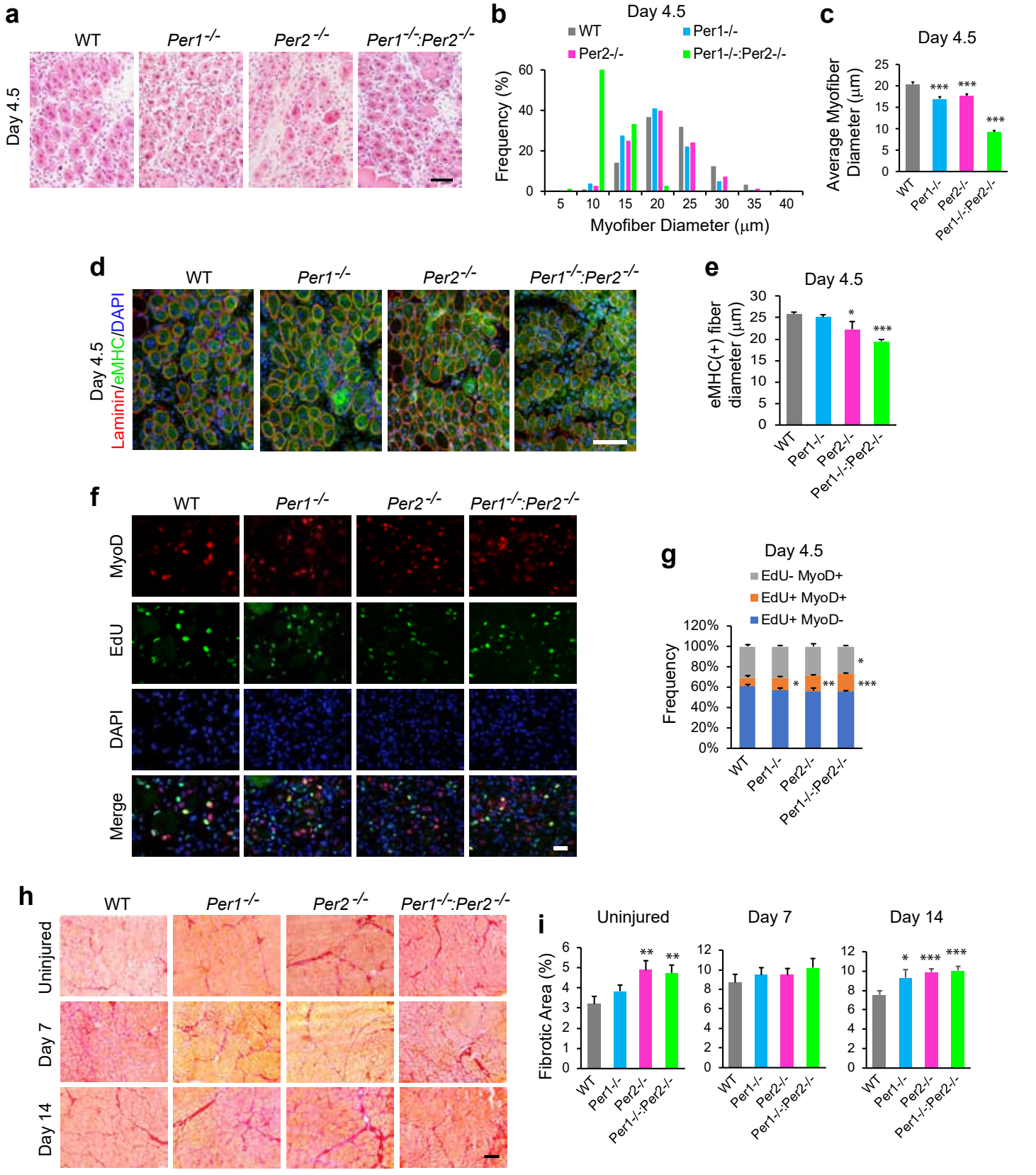

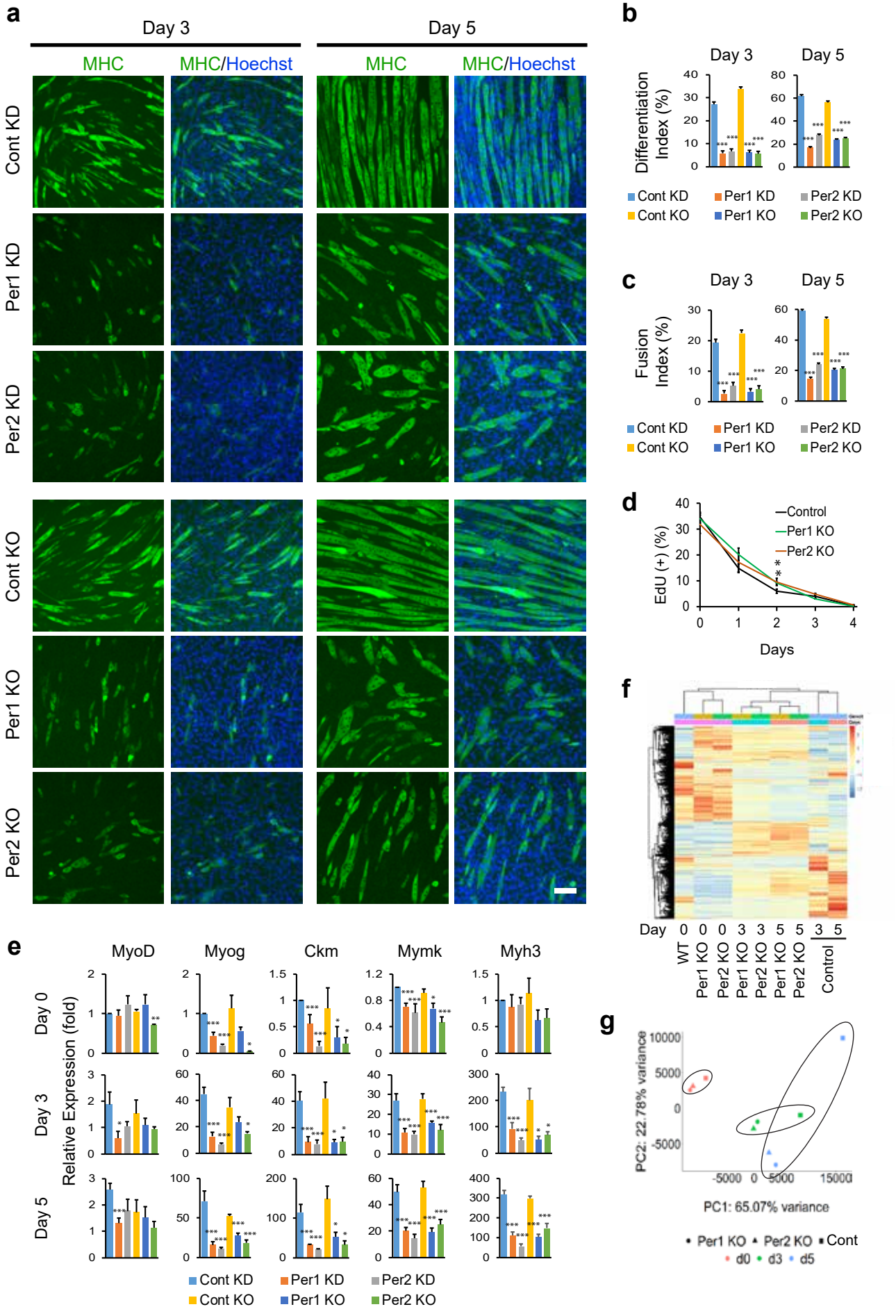

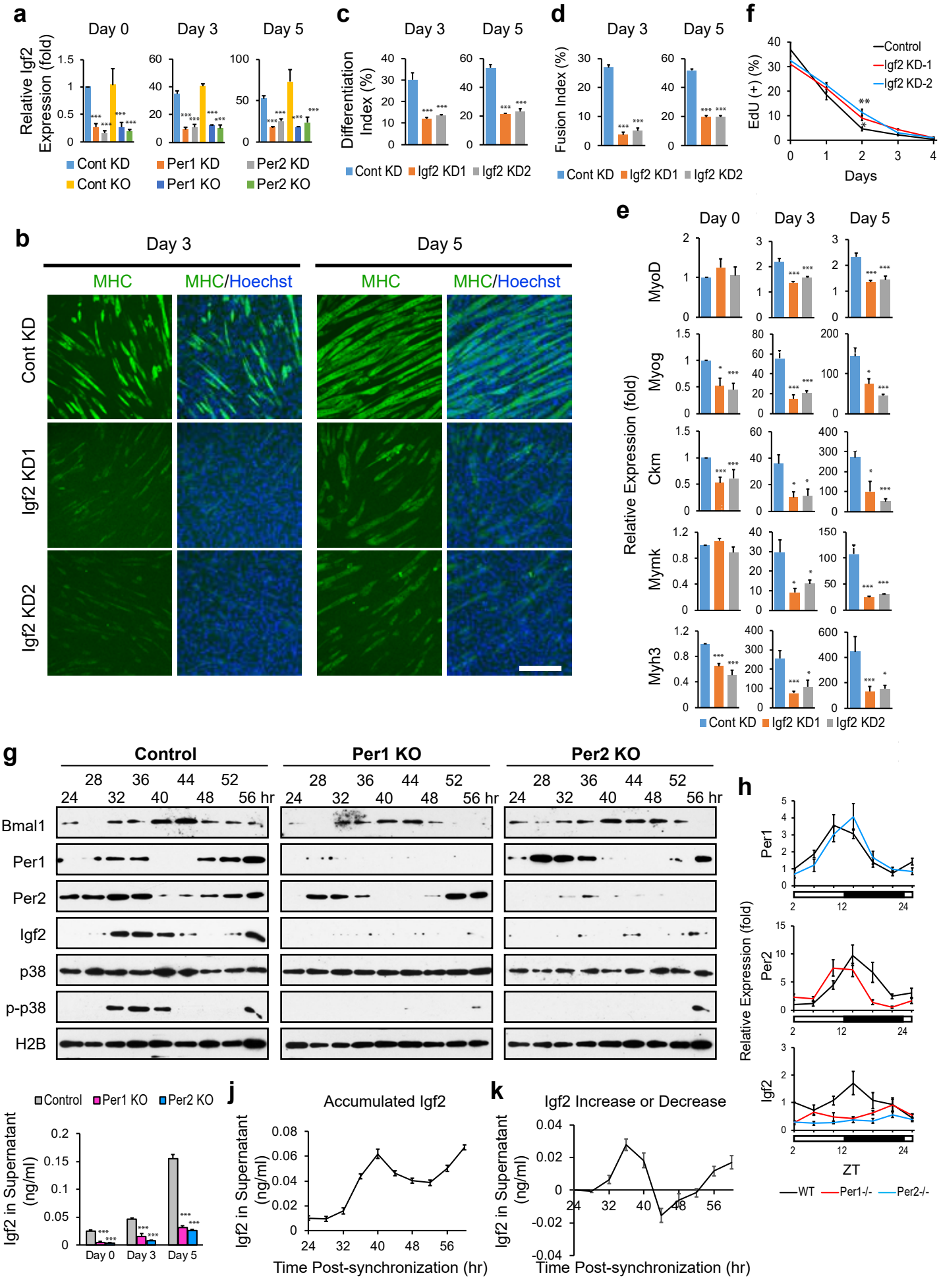

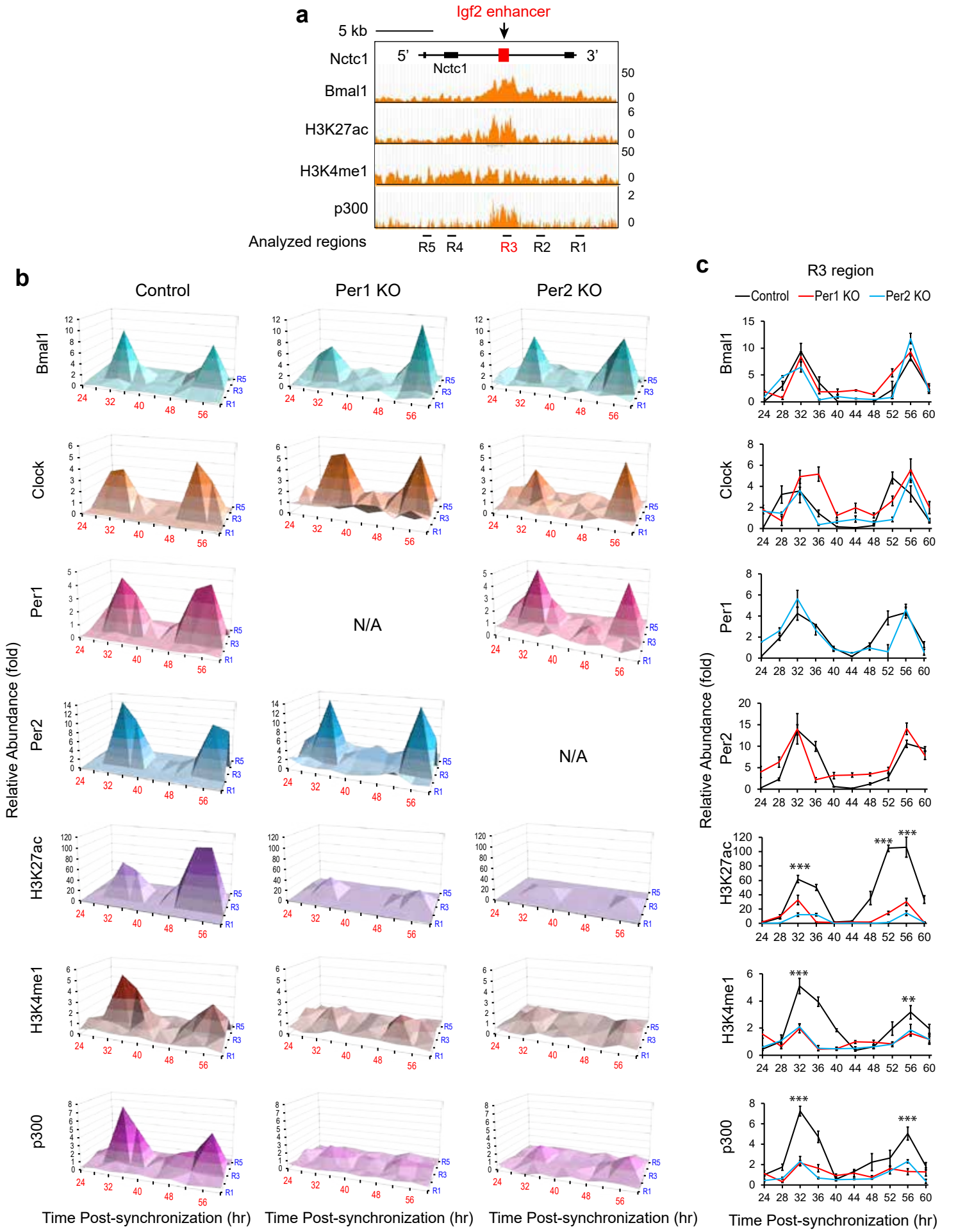

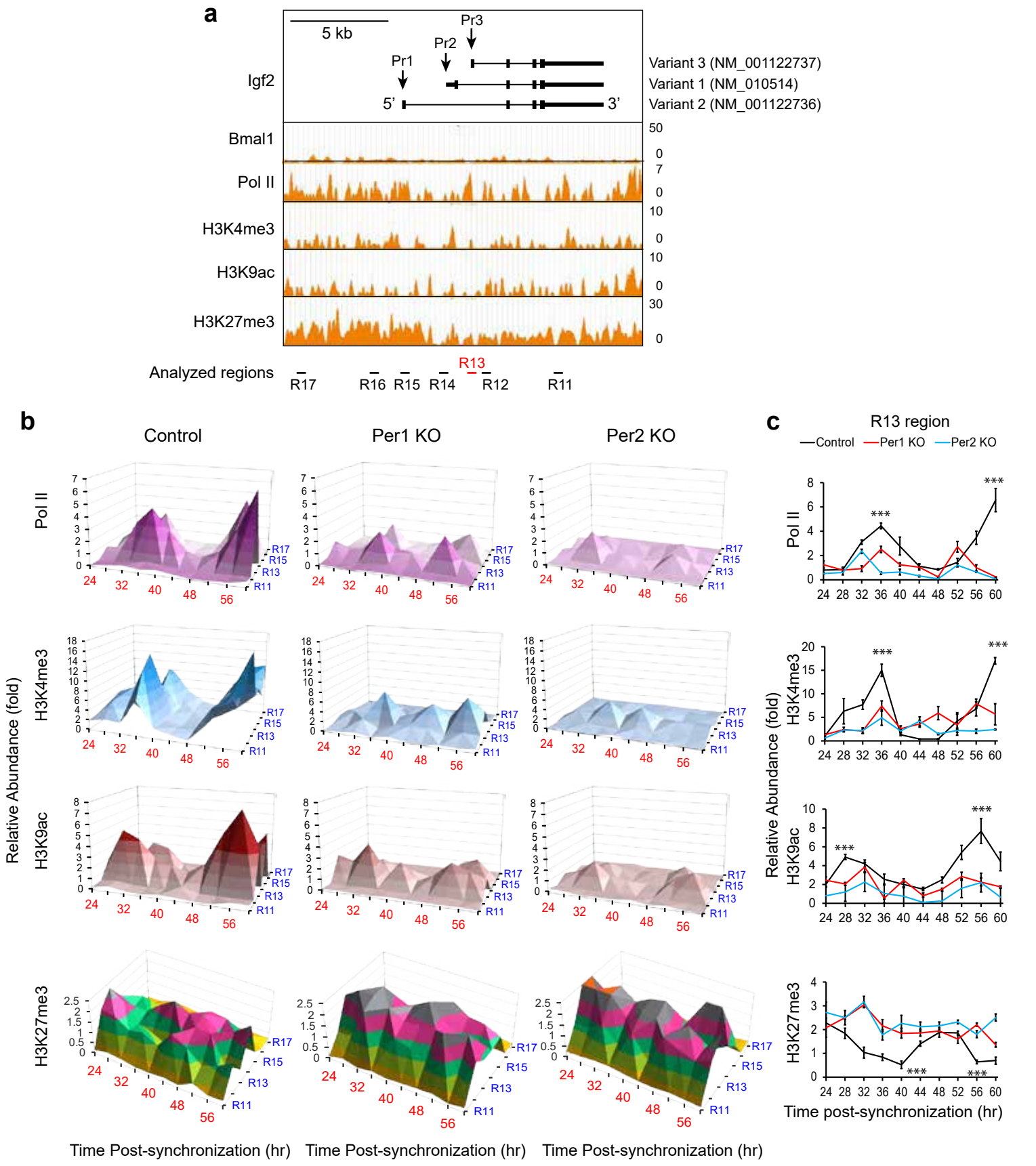

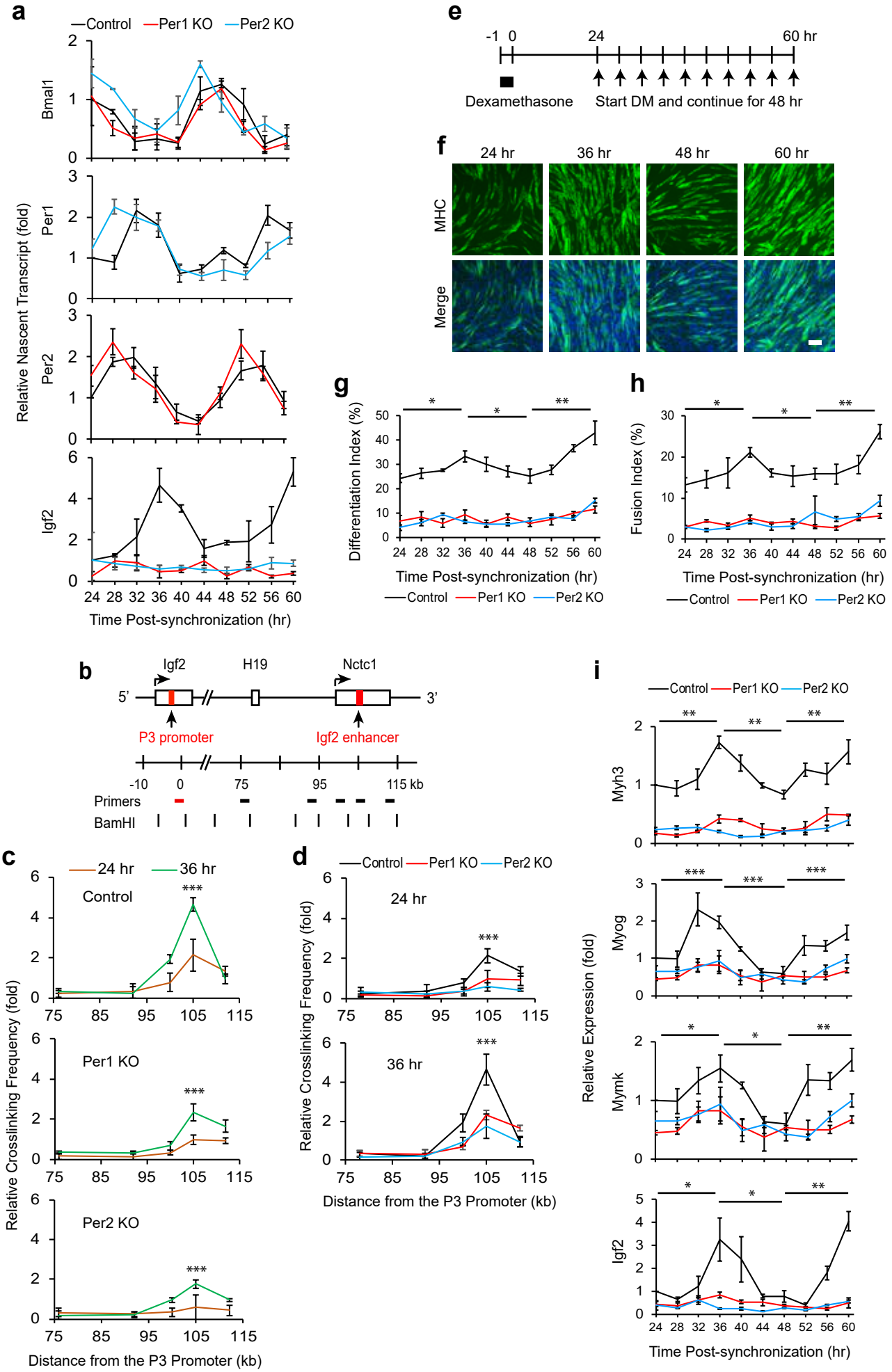

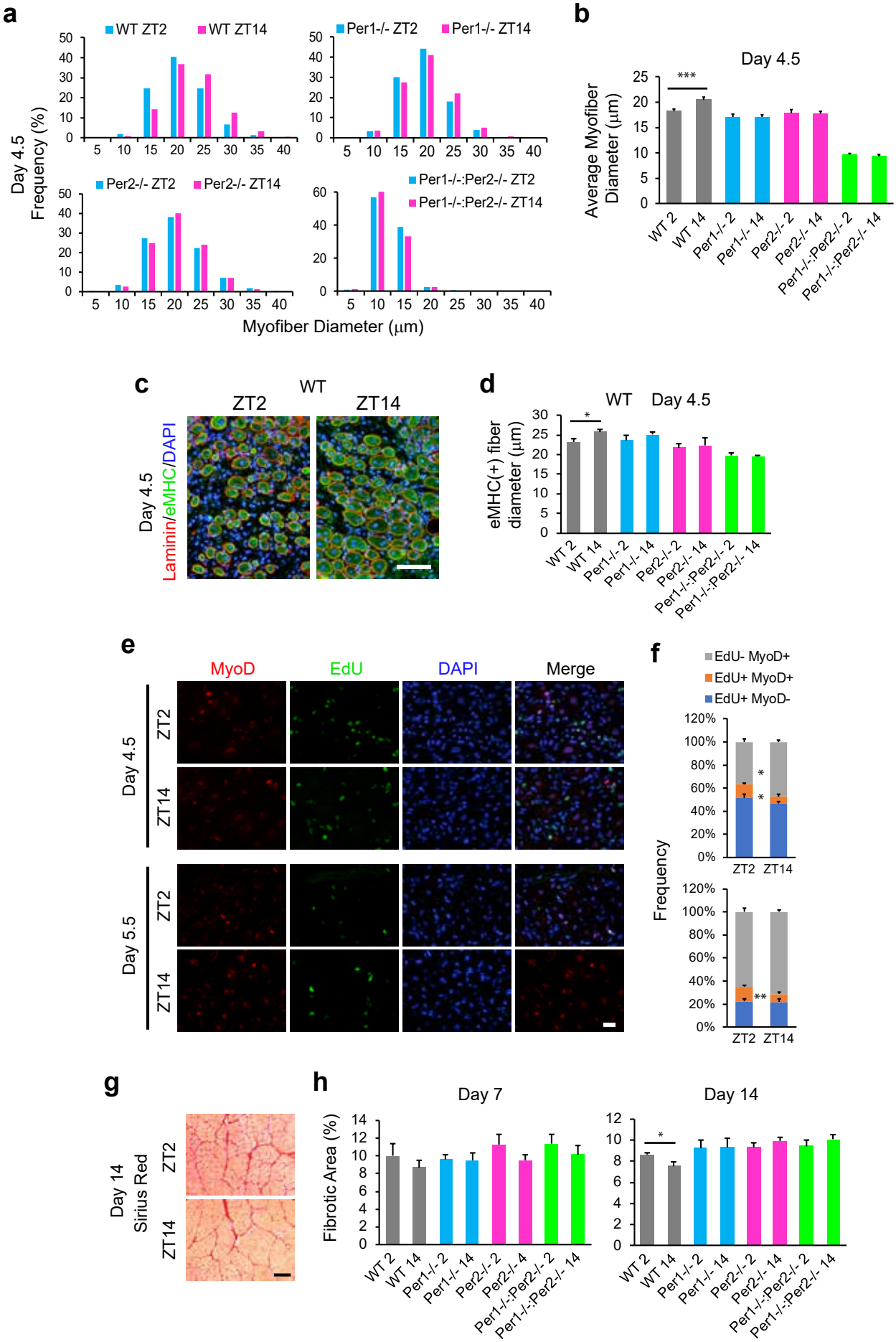

Supplementary Figure Legends

Supplementary Fig. 1. Regeneration of TA muscle and myoblast differentiation comparing *Per1*$^{-/-}$, *Per2*$^{-/-}$, and *Per1*$^{-/-}$:*Per2*$^{-/-}$ mice.

a, Average of the minimal Feret's diameters of myofibers with centrally-located nuclei on day 14. TA muscle was injured with barium chloride at ZT14 on day 0 and harvested 14 days later. n=8 mice with 4 males and 4 females in each group in **a** and **b**.

b, Average of the minimal Feret's diameters of myofibers in uninjured mice.

c-f. Immunofluorescence staining of undifferentiated (**c**) and differentiating primary myoblasts on day 1 (**d**), day 2 (**e**), and day 3 (**f**) with antibodies against MHC and MyoD. DNA was counterstained with DAPI. Bar, 100 μm.

g, Frequency of cells positive for EdU uptake and MHC expression during differentiation of primary myoblasts. n = 3 mice.

* $p < 0.05$, ** $p < 0.01$, and *** $p<0.001$ with Student's t-test in comparison to WT mice. Data are presented as mean + SEM in **a**, **b**, and **g**.

Supplementary Fig. 2. Comparison of transcriptomes between control and Per-depleted C2C12 cells.

a, Relative expression levels of *Per1* and *Per2* mRNAs in C2C12 cells after KD of each gene. The expression level with control scrambled shRNA was defined as 1.0 for each gene. *** $p<0.001$ with Student's t-test. Data are presented as mean + SEM of n=3 biological replicates.

b, Indel frequency in *Per1* KO and *Per2* KO C2C12 cells analyzed with the TIDE software (https://tide.nki.nl/).

c, Venn diagrams displaying the number of genes whose expression levels were >200% or <50%

of those of control cells.

d, The number of genes that were commonly up- (Cont > x 2) or down-regulated (Cont < x 0.5) in *Per1* KO and *Per2* KO cells compared with control KO cells.

e, Scatter plots comparing control, *Per1* KO, and *Per2* KO C2C12 cells.

f, Gene ontology (GO) terms relevant to muscle differentiation that were enriched in the genes commonly downregulated in *Per1* KO and *Per2* KO cells compared with control KO cells.

Supplementary Fig. 3. RNA-seq analysis of *Per1* and *Per2* KD cells.

a, List of genes belonging to the GO terms shown in Supplementary **Fig. 2f**. *Igf2* is highlighted in yellow.

b, Expression level of *Igf2* mRNA (CPM: count per million reads) taken from the RNA-seq analysis.

c, Relative expression level *Igf2* mRNA after KD with shRNA. The expression level with control scrambled shRNA was defined as 1.0. *** $p<0.001$ with Student's t-test. Data are presented as mean + SEM of n=3 biological replicates.

Supplementary Fig. 4. Promoted differentiation of C2C12 cells by Igf2

a-**d**, Differentiation index (**a**), fusion index (**b**), and relative expression of *Myog* and *Ckm* (**c**, **d**) of control, *Per1* KO, and *Per2* KO C2C12 cells with various concentrations of Igf2. The expression level of control KD cells before differentiation was defined as 1.0 in **c** and **d**. * $p < 0.05$, ** $p < 0.01$, and *** $p<0.001$ with Student's t-test in comparison to the value at 0 ng/ml Igf2. Data are presented as mean ± SEM of n=3 biological replicates in **a**-**d**.

Supplementary Fig. 5. ChIP analyses of the *Igf2* enhancer

a, ChIP-PCR analyses of indicated proteins in control and *Per* KO C2C12 cells. The graphs in **Fig. 4b** are shown from a different angle here to highlight the peaks specific to the R3 region. Data are presented as mean of n=3 biological replicates.

Supplementary Fig. 6. Expression analysis of the *Igf2* variants and ChIP analyses of the *Igf2* promoter

a, Locations of the PCR primers specific to two variants and common to all three variants of *Igf2*.

b, qRT-PCR results of the Igf2 variants in control and *Per* KO cells. The PCR products obtained with the common primers largely represented the expression levels of variant 3 because the levels of variants 1 and 2 were by far lower than the level of variant 3. Data are presented as mean ± SEM of n=3 biological replicates.

c, ChIP-PCR analyses of indicated proteins in control and *Per* KO C2C12 cells. The graphs in **Fig. 5b** are shown from a different angle here to highlight peaks specific to the R13 and R15 regions. Data are presented as mean of n=3 biological replicates.

Supplementary Fig. 7. Differential efficiency of myoblast differentiation and muscle regeneration depending on circadian timing

a-c, Analyses of differentiation index (**a**), fusion index (**b**), and relative expression of differentiation-specific genes (**c**) with C2C12 cells that were induced to differentiate at the indicated post-synchronization time points. Control and *Igf2* KD cells prepared with two shRNA clones were compared.

d, Average diameters of myofibers with centrally-located nuclei on day 14. TA muscle was injured

with barium chloride at ZT2 or ZT14 on day 0 and harvested 14 days later. n=8 mice with 4 males and 4 females in each group. 2 and 14 at the end of each genotype indicate the injury time at ZT2 and ZT14, respectively.

* $p < 0.05$, ** $p < 0.01$, and *** $p<0.001$ with Student's t-test comparing two time points. **a-c** show mean ± SEM of n=3 biological replicates.

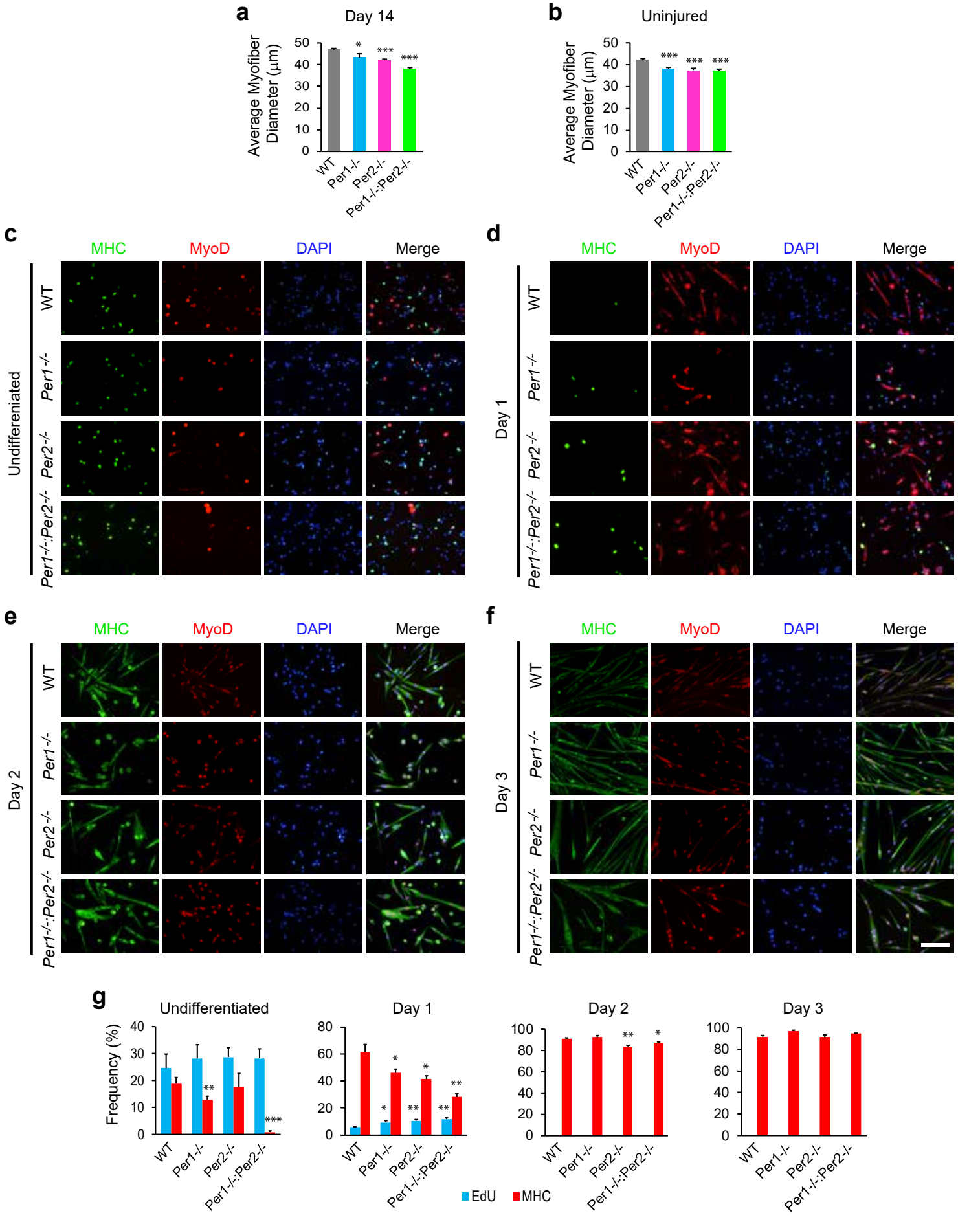

a

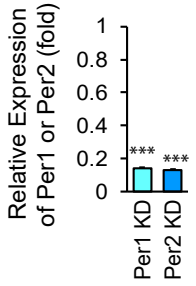

b

Per1 KO		Per2 KO	
Base number of Insertion or deletion	Frequency (%)	Base number of Insertion or deletion	Frequency (%)
3	0.2	3	0
2	5.2	2	1.1
1	41.8	1	49.7
0	15.1	0	18.4
-1	10.3	-1	2.1
-2	11.2	-2	2.3
-3	5.2	-3	1.3
-4	1.2	-4	4.1
-5	0	-5	5.2
Others	9.8	Others	15.8
Total frameshift	**79.1**	**Total frameshift**	**79**

c

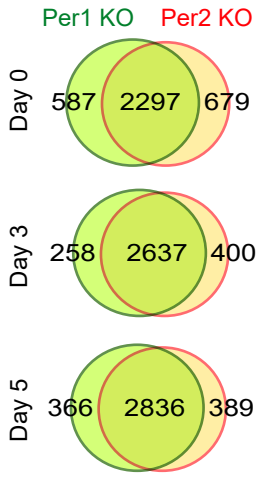

e

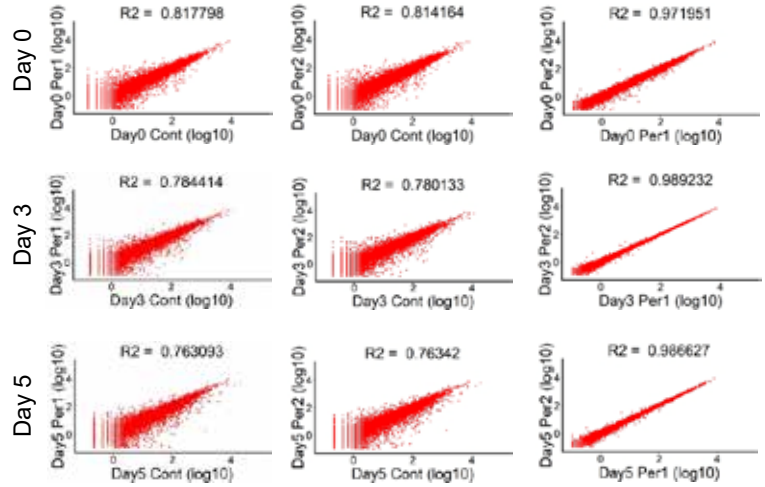

d

	> Cont x 2	< Cont x 0.5
Day 0	1095	1202
Day 3	1343	1294
Day 5	1424	1412

f

GO biological process: muscle differentiation	Log2 FC	Q-value
Day 0		
muscle filament sliding (GO:0030049)	13.11	2.56E-02
actin-myosin filament sliding (GO:0033275)	12.74	8.01E-03
skeletal muscle thin filament assembly (GO:0030240)	12.35	7.73E-04
skeletal muscle adaptation (GO:0043501)	11.47	3.46E-02
skeletal myofibril assembly (GO:0014866)	11.47	1.01E-03
striated muscle myosin thick filament assembly (GO:0071688)	10.19	4.48E-02
skeletal muscle myosin thick filament assembly (GO:0030241)	10.19	4.47E-02
regulation of skeletal muscle contraction (GO:0014819)	8.82	2.28E-02
sarcomere organization (GO:0045214)	8.67	1.05E-07
myofibril assembly (GO:0030239)	8.24	2.86E-10
Day 3		
skeletal muscle contraction (GO:0003009)	8.25	7.57E-05
positive regulation of myotube differentiation (GO:0010831)	6.87	1.12E-04
positive regulation of myoblast differentiation (GO:0045663)	6.45	5.24E-03
positive regulation of myoblast fusion (GO:1901741)	5.93	3.10E-02
sarcomere organization (GO:0045214)	5.8	4.23E-04
myofibril assembly (GO:0030239)	5.44	3.56E-05
regulation of myoblast fusion (GO:1901739)	5.22	4.68E-02
regulation of myotube differentiation (GO:0010830)	5.18	1.15E-04
regulation of myoblast differentiation (GO:0045661)	4.91	3.83E-04
myotube cell development (GO:0014904)	4.76	3.54E-02
Day 5		
muscle cell proliferation (GO:0033002)	6.51	3.62E-03
striated muscle cell proliferation (GO:0014855)	6.51	1.83E-02
positive regulation of myoblast fusion (GO:1901741)	6.21	1.01E-02
positive regulation of myotube differentiation (GO:0010831)	6.17	1.69E-04
regulation of skeletal muscle cell differentiation (GO:2001014)	5.86	2.63E-02
regulation of myoblast fusion (GO:1901739)	5.47	1.67E-02
regulation of myotube differentiation (GO:0010830)	4.34	7.20E-04
positive regulation of striated muscle cell diff (GO:0051155)	4.28	2.45E-04
skeletal muscle tissue regeneration (GO:0043403)	4.14	4.89E-02
positive regulation of muscle cell differentiation (GO:0051149)	3.99	1.62E-04

a

Downregulated muscle genes in Per1 KO cells and Per2 KO cells

Day 0

	Per1 KO		Per2 KO	
Gene	log2 FC	Q-value	log2 FC	Q-value
Acta1	-4.5232	3.68E-17	-6.0788	2.88E-26
Actc1	-5.54246	5.08E-22	-6.85725	1.03E-28
Actn2	-5.57798	4.66E-08	-9.1953	2.01E-10
Ar	-1.34555	0.032888	-1.62824	0.005646
Atp2a1	-3.1236	3.27E-09	-3.44497	9.13E-11
Cacna1s	-4.93404	1.22E-14	-5.86566	1.09E-17
Casq2	-3.84794	1.56E-12	-4.35672	3.58E-15
Cav3	-5.88124	2.89E-06	-8.61157	1.36E-07
Cmya5	-5.32246	0.246938	-5.32246	0.230834
Csrp3	-3.16886	0.005969	-4.71021	0.000168
Dbn1	-1.04682	0.120959	-1.14704	0.071728
Igf2	-4.63907	5.96E-15	-5.72011	2.84E-19
Kcnj2	-2.54982	2.84E-06	-3.50722	1.49E-10
Klhl41	-2.61457	1.44E-06	-3.68377	1.96E-11
Krt19	-1.08595	0.106923	-1.07887	0.106654
Lmod2	-3.95407	1.08E-07	-4.44435	6.42E-09
Lmod3	-2.09717	0.000323	-2.39799	2.85E-05
Mybpc1	-6.88318	0.008568	-6.88318	0.007971
Myh6	-6.30432	0.047303	-6.30432	0.045482
Myh7	-4.67324	0.0002	-8.29056	2.42E-06
Myh8	-4.19143	5.21E-05	-8.74874	3.37E-08
Myom1	-2.95985	1.03E-06	-3.5975	4.64E-09
Myom2	-1.88002	0.000592	-1.0854	0.103354
Myom3	-3.66673	5.00E-09	-4.93412	3.03E-13
Myoz1	-1.35684	0.620973	-3.30283	0.11559
Myoz2	-4.00706	4.63E-05	-4.04595	3.70E-05
Mypn	-2.59778	0.02477	-8.29056	2.42E-06
Neb	-2.61984	2.04E-06	-3.36942	1.16E-09
Pdgfra	-1.62486	0.005807	-1.56806	0.008226
Pgm5	-4.57429	9.99E-11	-4.03755	3.02E-09
Scn4a	-2.12136	0.103517	-3.97404	0.001809
Tmod1	-1.84691	0.001648	-2.09619	0.000248
Tnnc1	-2.93727	2.36E-08	-3.74516	2.22E-12
Tnni1	-3.3754	1.38E-10	-4.65912	1.92E-17
Tnnt2	-1.28918	0.034558	-2.09116	8.01E-05
Tnnt3	-2.95981	2.07E-08	-4.05668	6.28E-14

Day 3

	Per1 KO		Per2 KO	
Gene	log2 FC	Q-value	log2 FC	Q-value
Acta1	-1.47051	0.010736	-1.67922	0.002257
Actc1	-2.30575	1.02E-05	-2.34985	6.50E-06
Actn2	-4.12858	7.72E-15	-4.22225	2.39E-15
Ankrd2	-1.34642	0.026763	-1.81189	0.001009
Ankrd23	-1.69932	0.022074	-2.06952	0.003125
Atp2a1	-1.2148	0.052377	-1.40362	0.01633
Boc	-1.03931	0.240092	-1.08511	0.193473
Cav3	-1.95517	0.00039	-1.99031	0.000279
Cd53	-1.79092	0.009639	-1.91059	0.004677
Chrng	-1.23492	0.046331	-1.36998	0.019993
Csrp2	-2.16535	4.90E-05	-2.21573	3.02E-05
Csrp3	-3.01311	7.58E-09	-3.29196	2.88E-10
Cxcl14	-2.0915	0.367287	-2.34676	0.272588
Ddit3	-1.05949	0.126927	-1.02684	0.13947
Gdf15	-1.62664	0.005597	-1.69041	0.003422
Igf2	-2.75477	9.62E-08	-2.89236	2.02E-08
Il4ra	-1.38004	0.021452	-1.24966	0.044389
Klhl40	-1.33442	0.028883	-1.50789	0.009211
Klhl41	-1.88134	0.000494	-1.97259	0.000221
Lmod2	-1.46162	0.012453	-1.39892	0.0179
Mamstr	-1.94266	0.010249	-2.21616	0.00242
Map3k5	-1.60015	0.26541	-1.33952	0.369848
Mybpc1	-2.42584	6.49E-06	-2.52592	2.44E-06
Myf6	-1.93278	0.316311	-1.02848	0.663598
Myh14	-1.00225	0.318251	-1.29869	0.123249
Myh3	-1.02328	0.13502	-1.1008	0.088672
Myog	-1.71325	0.001893	-1.92334	0.000328
Myoz1	-1.6735	0.233156	-1.67383	0.217013
Myoz2	-1.61212	0.00451	-1.83646	0.000796
Mypn	-2.34993	4.42E-05	-2.45704	1.81E-05
Neu2	-2.14214	0.001446	-1.80809	0.009211
Nfatc2	-2.19409	0.044408	-2.57696	0.014532
Nmrk2	-1.33112	0.04883	-1.7285	0.00461
Pgm5	-2.08996	9.32E-05	-2.03121	0.000156
Rbm24	-2.23354	2.33E-05	-2.38633	5.37E-06
Scn4a	-1.04417	0.149478	-1.26647	0.049883
Smyd1	-1.28677	0.035498	-1.51173	0.008196
Stac	-3.30844	0.006129	-5.7039	5.68E-05
Stac3	-1.14532	0.081328	-1.32349	0.029812
Tcap	-1.57759	0.01977	-2.45777	6.01E-05
Tgfb1	-1.12775	0.086367	-1.21381	0.053514
Tmem119	-1.53766	0.007158	-1.81142	0.000888
Tmod1	-1.49253	0.010432	-1.69354	0.002358
Tnnc1	-1.0618	0.112277	-1.21023	0.05089
Tnni2	-1.54142	0.006585	-1.72641	0.00161
Tnnt2	-1.13628	0.07793	-1.18665	0.057863
Tnnt3	-1.0049	0.147576	-1.10415	0.087659
Trim72	-1.51198	0.008646	-1.7015	0.002073

Day 5

	Per1 KO		Per2 KO	
Gene	log2 FC	Q-value	log2 FC	Q-value
Akr1b3	-1.13846	0.074194	-1.06359	0.106544
Bcl9	-1.32967	0.034622	-1.22248	0.061129
Bdnf	-1.78962	0.001309	-1.74919	0.00174
Capn3	-1.20105	0.062793	-1.33555	0.029907
Cav1	-1.49907	0.008205	-1.25841	0.036795
Cav3	-1.15771	0.067523	-1.61755	0.003997
Cd53	-1.83362	0.008744	-1.8139	0.009792
Csrp3	-2.6553	3.08E-07	-3.00128	6.97E-09
Cth	-4.98732	1.08E-18	-5.01479	9.38E-19
Cx3cl1	-1.37972	0.027648	-1.41839	0.021931
Cxcl12	-2.81713	6.53E-08	-1.8842	0.000516
Dysf	-1.1324	0.075009	-1.4104	0.015481
Ednra	-1.9846	0.000309	-1.98667	0.000303
Ephb1	-7.92055	0.000659	-7.92055	0.000677
Esr1	-1.68492	0.0034	-1.19546	0.064943
Foxc1	-1.66455	0.004492	-1.59051	0.00738
Foxc2	-1.04425	0.189811	-1.01057	0.215551
Gata6	-1.50638	0.329221	-1.03726	0.590708
Gdf15	-3.14538	2.13E-09	-2.86778	4.83E-08
Gja1	-1.47415	0.009896	-1.31093	0.027712
Gper1	-2.02797	0.000451	-2.02308	0.000472
Hbegf	-1.01412	0.15677	-1.39841	0.023661
Hmox1	-1.33326	0.026597	-1.27515	0.036671
Hopx	-4.12102	1.10E-11	-2.88301	9.23E-07
Hpgd	-3.6435	7.05E-10	-4.61897	9.09E-14
Igf2	-2.48958	1.52E-06	-2.60649	4.43E-07
Il4ra	-1.39498	0.017383	-1.30245	0.030317
Itgb3	-1.48957	0.011181	-1.38024	0.021909
Kalrn	-1.21442	0.082422	-1.10368	0.131874
Kcnk2	-1.19749	0.241102	-1.2008	0.23809
Mamstr	-2.47173	0.000473	-1.98407	0.006657
Map3k5	-1.35995	0.533857	-1.8198	0.327009
Mmp2	-4.56831	6.85E-18	-3.92931	4.63E-14
Myc	-1.19962	0.057392	-1.21388	0.052828
Myf6	-2.98506	0.000295	-3.58673	2.00E-05
Myog	-1.57665	0.00461	-1.95264	0.000231
Myoz1	-1.20048	0.267473	-1.75079	0.05588
Ndrg2	-1.64405	0.004162	-1.76736	0.001687
Nfatc2	-3.14508	0.014603	-2.55245	0.050339
Npr3	-1.31356	0.05906	-1.61547	0.012214
Nrg1	-2.60253	2.07E-06	-2.38439	1.53E-05
Pax7	-1.14697	0.194799	-1.17024	0.182917
Pde1a	-2.87806	1.18E-05	-3.15085	1.81E-06
Ptgfrn	-1.31239	0.026293	-1.25076	0.037104
Ptgs2	-1.10647	0.092869	-1.13438	0.080625
Rbfox1	-2.80008	4.51E-07	-3.32117	2.52E-09
Rbm24	-1.76161	0.001252	-2.23387	2.03E-05
Tbx1	-1.24586	0.063542	-1.16084	0.093566
Tcf7l2	-2.08785	0.000569	-1.69655	0.007456
Tenm4	-1.88563	0.00139	-1.67337	0.005822
Tgfbr3	-1.52663	0.009635	-1.33758	0.029808
Tmem119	-1.59122	0.00442	-1.66852	0.002501
Vegfa	-1.15513	0.064723	-1.08663	0.090769

b

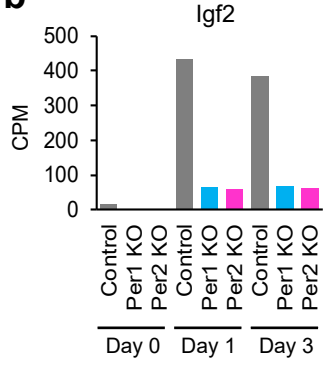

c

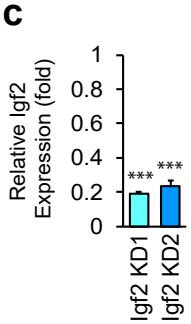

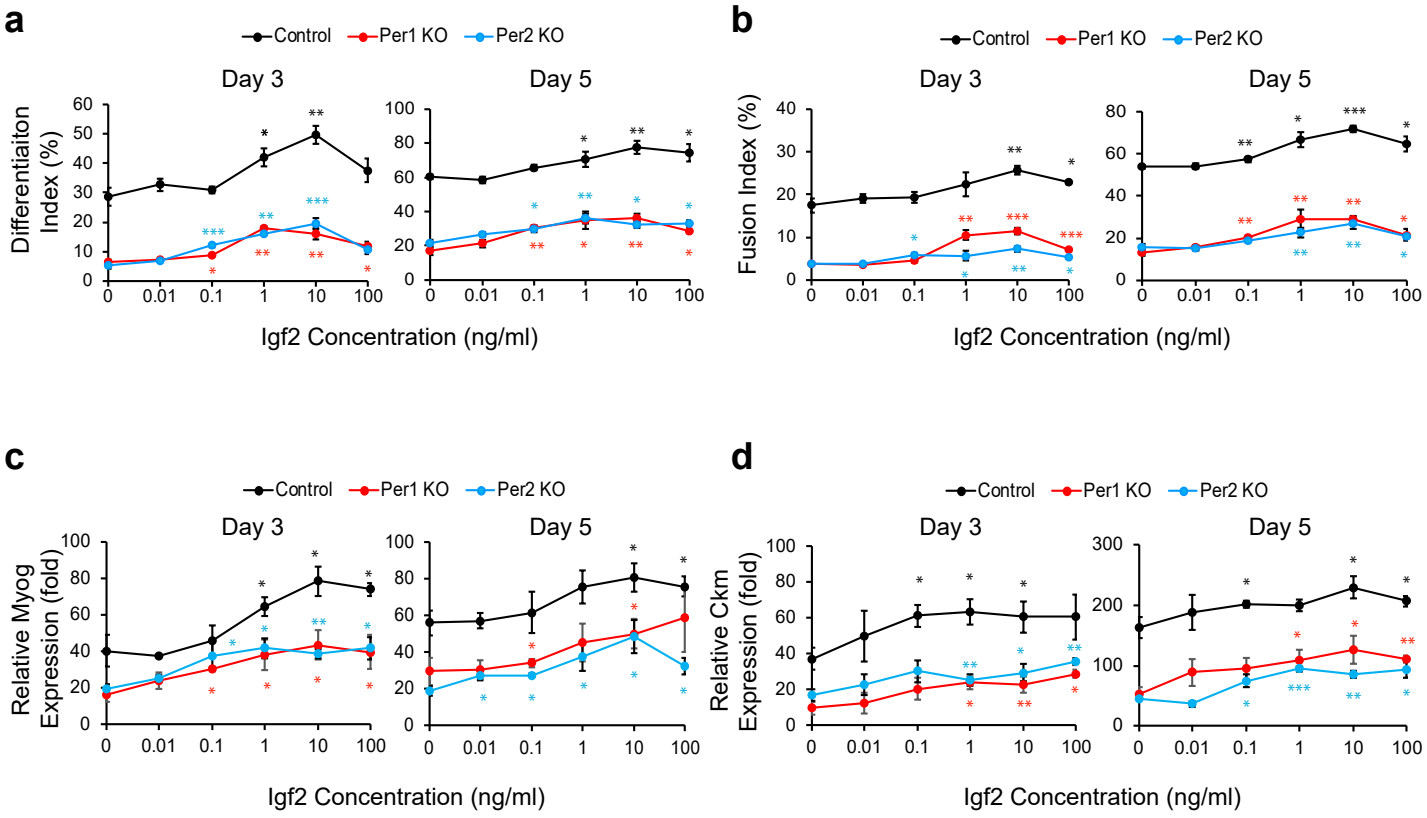

a

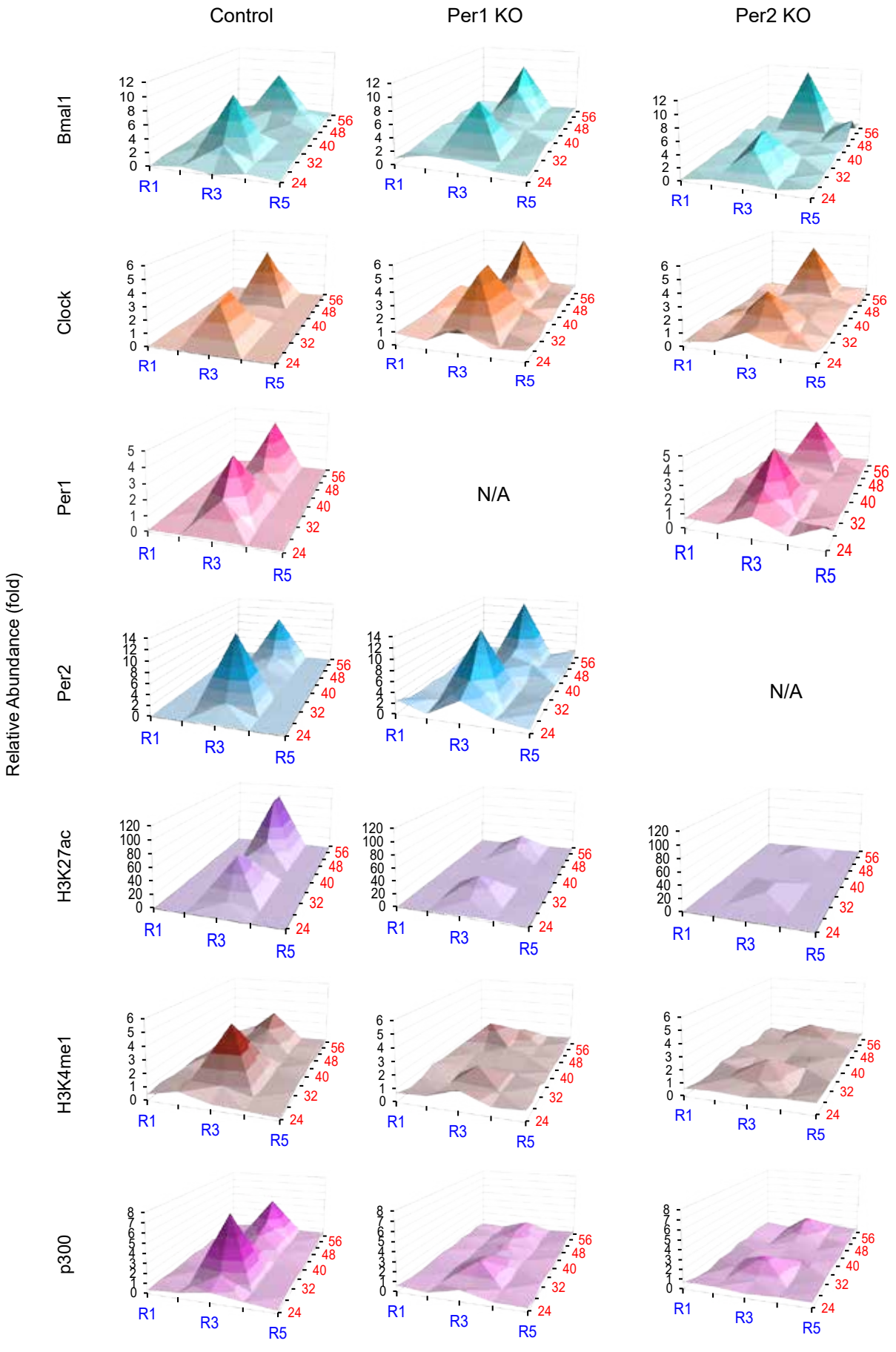

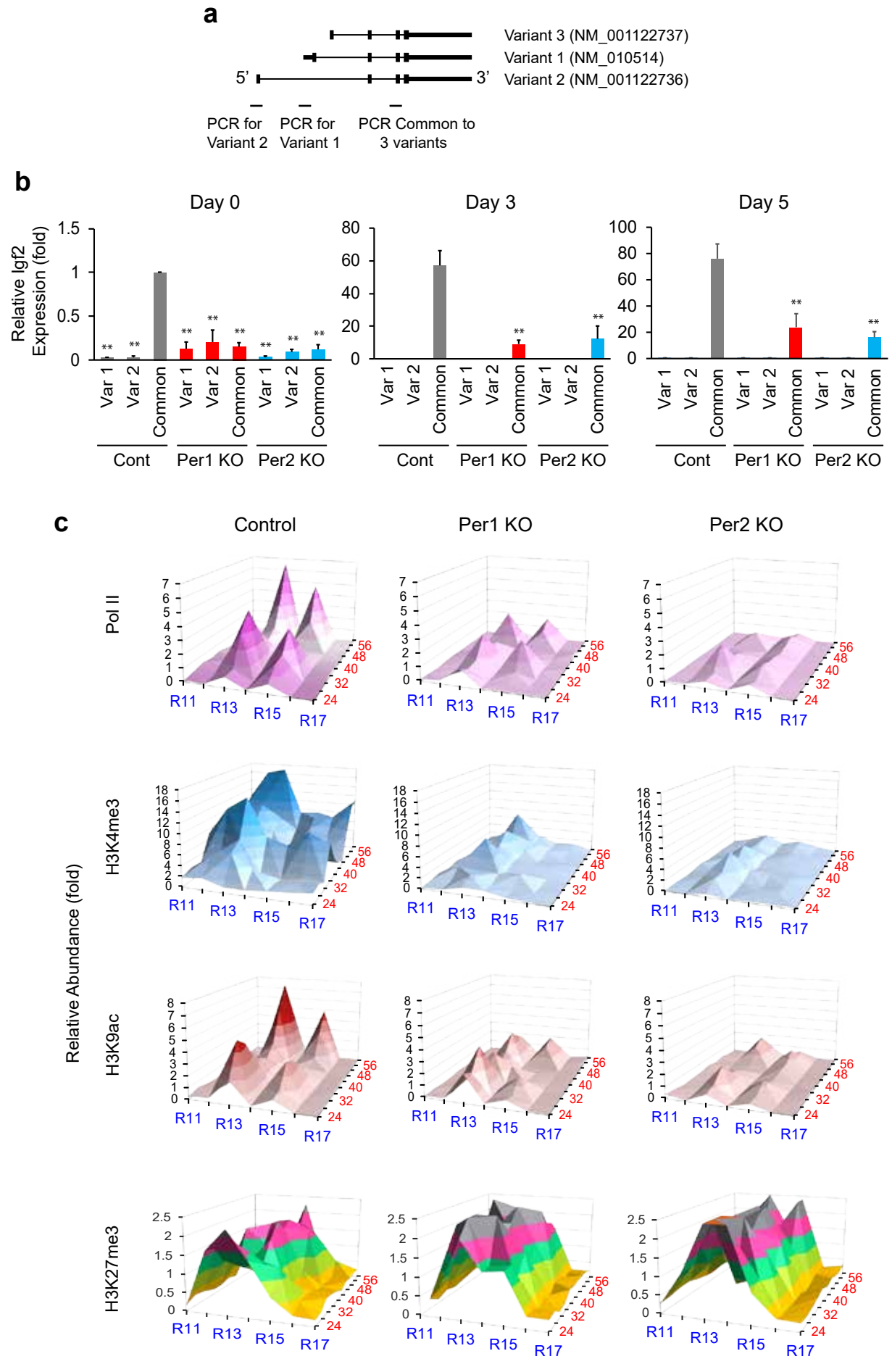

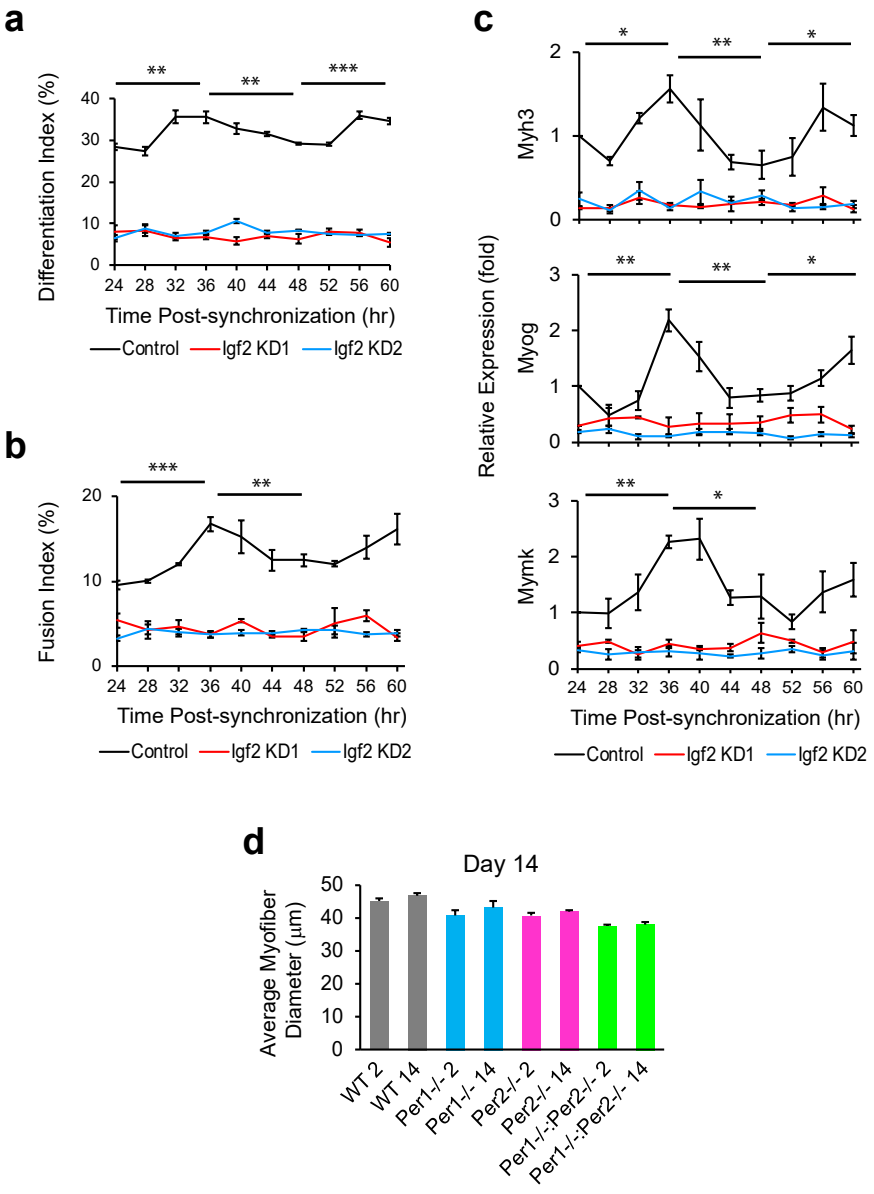

Supplementary Table S1. shRNA and sgRNA sequences

shRNA clones		
Gene	**Manufacturer**	**Catalog #**
Control	MilliporeSigma	SHC016-1EA
Per1	GE Life Sciences	TRCN0000023176
Per2	GE Life Sciences	TRCN0000000364
Igf2-1	GE Life Sciences	TRCN0000111861
Igf2-2	GE Life Sciences	TRCN0000111862
sgRNAs		
Gene	**Manufacturer**	**Sequence**
Control	Synthego	GCACUACCAGAGCUAACUCA
Per1	Synthego	ACAUGAGUGGUCCCCUAGAA
Per2	Synthego	AUUCCAGAGCCCGACAUGAA

Supplementary Table 2. Antibodies

Protein	Manufacturer	Catalog #	Dilution (fold)
CD31-PE	eBioscience	12-0311	200
CD45-PE	eBioscience	12-0451	200
Sca1-PE	eBioscience	12-5981	200
Integrin α7-biotin	Miltenyi Biotec	130-102-125	200
Laminin	MilliporeSigma	L0663	1000
Bmal1	Abcam	Ab3350	200
Clock	Abcam	Ab3517	200
Per1	MilliporeSigma	AB2201	100
Per2	NOVUS	NB100-125	100
Igf2	Santa Cruz Biotechnology	sc-5622	100
p38α/β	Santa Cruz Biotechnology	sc-7972	300
p-p38	Thermo Fisher Scientific	MA5-15177	400
Histone H2B	Thermo Fisher Scientific	MA5-14835	1000
H3K27ac	MilliporeSigma	07-360	500
H3K4me1	MilliporeSigma	07-436	500
H3K4me3	MilliporeSigma	07-473	500
H3K9ac	MilliporeSigma	07-352	400
H3K27me3	MilliporeSigma	07-449	400
p300	MilliporeSigma	05-257	300
Pol II, CTD	MilliporeSigma	05-952-I-100UG	600
Embryonic MHC	Developmental Studies Hybridoma Bank	F1.652	50
MHC	Developmental Studies Hybridoma Bank	MF 20	50

MyoD	Santa Cruz Biotechnology	sc-304	500
Alexa Fluor 488 goat anti-mouse IgG	Thermo Fisher Scientific	A-11029	1000
Alexa Fluor 488 donkey anti-mouse IgG	Thermo Fisher Scientific	A-21202	1000
Alexa Fluor 594 donkey anti-rat IgG	Thermo Fisher Scientific	A-21209	1000
Alexa Fluor 594 donkey anti-rabbit IgG	Thermo Fisher Scientific	A-21207	1000
Goat anti-mouse IgG, HRP labeled	Santa Cruz Biotechnology	sc-2005	1000
Goat anti-rabbit IgG, HRP labeled	Santa Cruz Biotechnology	sc-2004	1000

Supplementary Table 3. Sequences of qPCR primers

Gene	Forward	Reverse
MyoD	TGAGCAAAGTGAATGAGGCCTTCG	TGCAGACCTTCGATGTAGCGGAT
Myogenin (*Myog*)	CCCTATTTCTACCAGGAGCCCCAC	GCGCAGGATCTCCACTTTAGGCAG
Myomaker (*Mymk*)	ATCGCTACCAAGAGGCGTT	CACAGCACAGACAAACCAGG
MHC3 (*Myh3*)	CACCTGGAGAGGATGAAGAAGAA	AAGACTTGACTTTCACTTGGAGTTTATC
Ckm	CTCAGCAAGCACAACAATCAC	GATGACATCGTCCAGAGTGAAG
Gapdh	TGCACCACCAACTGCTTAG	GATGCAGGGATGATGTTC
Igf2	TACCTCTCAGGCCGTACTT	ACTGTCTCCAGGTGTCATATTG
Bmal1	CAACCCATACACAGAAGCAAAC	CATCTGCTGCCCTGAGAATTA
Per1	CAGGATGTGGGTGTCTTCTATG	GTGAAGTCCTTGAGACCTGAAC
Per2	CAACAACCCACACACCAAAC	CTCGATCAGATCCTGAGGTAGA
ChIP R1	CCTTCTCTTCTGCCTCTCTTTG	AAACAACCTGCTCCTGGATAG
ChIP R2	AGCGATTACAGGGTTTCTACAT	CCTTCCTCTCCAGGTGTTATTT
ChIP R3	CTGCGATGAGGCAGTCTAAA	GTGAAGACAGGCCAAGATGA
ChIP R4	CCCACTCCTATCCTTGCATTT	GGCTGGCCTTGATGTTTCTA
ChIP R5	CTCTCAGGGTGTGTGTGAATAC	GCCCTGAAAGGCTAGCTAAA
ChIP R11	ACACTAAAGGTGCTTGGGATAA	TCCCAGAACCCAAGAAGAAAG
ChIP R12	CCCTTGACCCTTCAGTTAAGTAG	CACTGGTCTCTCACATGTTTCT
ChIP R13	GGAAGAGGATGAAGACAGGAAA	GAGGAGCCACTCAGACATAAA
ChIP R14	GGCGTCTCTTCTGCTTCTTT	GCTGACCTCATTTCCCGATAC
ChIP R15	TTTGCAGAGTGCACACAAAG	CTACCTCGCAGTTTGTCCTC

ChIP R16	TCAGGGCCAGTCTCTACATTAC	CCACACACACACACACACTATC
ChIP R17	GGGAAGAAGTCACTACCTGAAC	CCACAGCAACCCTTACTTACT
3C-Clock1	CACTTTATTCCTGTCACCACTCGGGCA	
3C-Clock2	TGTGAGCATCTACTTCTGTATTTGCCAGGC	
3C-0 kb	TAAGAGATGATAGGTGTCTTTGGTGGGGCC	
3C-76 kb	AACCCCATAGCCATAAAAGCAGAGGCTG	
3C-92 kb	TTGACTACTACTGTGGGGCCCAACTATC	
3C-100 kb	GGTTAAACCTCTATGCTCCTCTCCAATGCC	
3C-105 kb	CCAGTGGGTTGCGTGTTTCTGATATCTG	
3C-112 kb	GTAACAAGGAGGCAACTGACCCTGTTTC	

Online Methods

Culture of C2C12 cells

Mouse myoblast C2C12 cells (American Type Culture Collection, CRL-1772) were maintained in the growth medium [10% fetal bovine serum (FBS) in Dulbecco's Modified Eagle Medium (DMEM)] in a 37°C and 5% CO_2 incubator. Differentiation was induced on day 0 when cells were at 90% confluence by rinsing with phosphate buffered saline (PBS) twice and adding the differentiation medium [5% horse serum (HS) in DMEM]. The medium was changed every two days thereafter. Concentration of endogenous Igf2 was measured with a mouse Igf2 ELISA kit (Thermo Fisher Scientific, EMIGF2). Because of the low Igf2 concentration, 300 µl culture supernatant was added seven times for 3 hr each (2.1 ml in total). The effect of exogenous Igf2 was tested with recombinant human IGF2 (Peprotech, 100-12). To synchronize circadian rhythms, C2C12 cells were seeded on day -1 and 0.2 µM dexamethasone was added at -1 hr on day 0. Cells were washed with PBS twice and fresh 10% FBS in DMEM was added at 0 hr. Cells were harvested for PCR or fixed for immunofluorescence staining every 4 hrs at indicated time points.

Gene Knockdown in C2C12 cells

On day 1, 293FT cells (Thermo Fisher Scientific, R70007) were seeded in DMEM with 10% FBS at $3x10^5$ cells/well in a 12-well plate. On day 2, cells were transfected with 0.5 µg pLKO.1 lentivirus vector encoding an shRNA sequence shown in Supplementary Table 1, along with 0.2 µg each of pCMV-VSV-G (Addgene, 8454), pRSV-Rev (Addgene, 12253), and pMDLg/pRRE (Addgene, 12251) using 2.75 µl Lipofectamine 2000 (Thermo Fisher Scientific, 11668019). The culture medium was replaced with fresh DMEM with 10% FBS 5 hr after transfection. On day 4, C2C12 cells were seeded at $1x10^5$ cells/well in 12-well plates. On day 5, culture supernatant of the

transfected 293FT cells was applied to a 0.45 μm syringe filter and added to C2C12 cells with 0.8 μg/ml polybrene (MilliporeSigma, H9268). The culture medium was replaced with fresh DMEM with 10% FBS on day 6. Virus-integrated cells were selected with 1 μg/ml puromycin dihydrochloride (MB Bio, 100552) between days 7 and 14. Selected cells were expanded and frozen in liquid nitrogen.

Gene Knockout in C2C12 cells

On day 1, C2C12 cells were seeded in DMEM with 10% FBS at $1.8x10^5$ cells/well in 12-well plates. Cells were transfected with 0.5 μg single guide RNA (sgRNA, Synthego) against *Igf2* (Supplementary Table 1), 0.5 μg CleanCap Cas9 mRNA (Cas9 mRNA, TriLink, L-7206), 0.2 μg CleanCap mCherry mRNA (TrLink, L-7203), and 1 μl TransIT (Mirus Bio TransIT-mRNA transfection kit, MIR-2225). More than 90% of the cells were mCherry (+) with fluorescence microscope observation on day 2. Cells were subcultured on day 3 to expand and freeze. A small aliquot of cells was used for Sanger sequencing of genomic DNA to verify the knockout efficiency.

Knockout Mice

All protocols were approved by the Institutional Animal Care and Usage Committee of the University of Minnesota (1902-36737A and 1903-36906A). *Per1*$^{+/-}$ mice (B6.129-*Per1*^{tm1Drw}/J, stock # 010491) and *Per2*$^{+/-}$ mice (B6.129-*Per2*^{tm1Drw}/J, stock# 010492) were purchased from Jackson Laboratory. *Per1*$^{-/-}$, *Per2*$^{-/-}$, *Per1*$^{-/-}$:*Per2*$^{-/-}$, and WT mice were obtained by breeding and identified by genotyping according to Jackson Laboratory protocols. The same number of male and female mice at the age of 8-10 weeks old were mixed in each group. Mice were entrained at 12 hr-light and 12 hr-dark cycles (6:00-18:00 light and 18:00-6:00 dark) for two weeks before

experiments. ZT0 corresponds to 6:00 and ZT12, 18:00. TA muscle was injected with 50 µl 1.2% $BaCl_2$ in 0.9% NaCl \at ZT2 or ZT14 to induce muscle injury and subsequent regeneration. Mice were euthanized on day 4.5, 7, and 14 after injury and the TA muscle was extracted at ZT2 or ZT14. In addition, uninjured TA muscle was isolated every 4 hr for qPCR. Mice were monitored by the Research Animal Resources staff of the University of Minnesota in specific pathogen free housing. Mice were given standard chow and access to drinking water without restrictions. Mice were euthanized via CO_2 inhalation. All methods align with the Panel of Euthanasia of the American Veterinary Medical Association recommendations.

Hematoxylin Eosin (HE) Staining

Cryosections of the TA muscle were fixed with 2% paraformaldehyde for 10 min. The sections were then treated as follows: deionized water for 1 min, Harris Modified Hematoxylin (Thermo Fisher Scientific, SH26-500D) for 2 min, tap water for 1 min, deionized water for 1 min, Eosin-Y (Thermo Fisher Scientific, 22-220-104) for 5 min, 95% ethanol for 30 sec, 100% ethanol for 2 min twice, and xylene for 10 min twice. The sections were mounted with Permount (Thermo Fisher Scientific, SP15-100). Images were captured with the cellSens Entry 1.11 software (Olympus) and a DP26 camera (Olympus) attached to an IX73 microscope (Olympus). The minimal Feret's diameter of each myofiber was quantified with Fiji (NIH).

Sirius Red Staining

The Sirius red solution was composed of 1% Direct Red 80 (MilliporeSigma, 365548) in 1.3% picric acid. TA sections were fixed with acetone, pre-chilled at -20°C, for 10 min. The sections were then washed in deionized water for 1 min, stained with Sirius red for 15 min, and rinsed with

0.5% acetic acid for 1 min. The sections were subsequently washed with 100% ethanol for 2 min and twice with xylene for 10 min. Finally, the sections were mounted with Permount for taking images as described for HE staining. Quantification of Sirius red (+) fibrotic was done using the entire section area with Fiji[1].

Immunofluorescence Staining of TA Sections

Sections were first fixed with 2% paraformaldehyde for 10 min, followed by permeabilization with 0.2% Triton X-100 in PBS for 5 min. The sections were treated with two blocking reagents: 3% Mouse-on-Mouse Blocking Reagent (Vector MKB-2213) in PBS for 1 hr and 10% bovine serum albumin (BSA) in PBS for 30 min. Primary antibodies against eMHC and laminin (see Supplementary Table 2 for catalog numbers) diluted in 10% BSA in PBS were applied overnight, followed by washing twice with 0.01% Triton-X100 in PBS. The secondary antibodies Alexa Fluor 488 donkey anti-mouse IgG and Alexa Fluor 594 donkey anti-rat IgG diluted in 10% BSA in PBS were used for 1 hr. DNA was counterstained with 4',6'-diamidine-2'-phenylindole dihydrochloride (DAPI, MilliporeSigma, 10236276001). Sections were mounted using Fluorescent Mounting Medium (DAKO, S302380-2). To label proliferating myoblasts, mice were intraperitoneally injected with 5-ethynyl-2'-deoxyuridine (EdU) at 50 μg/g body weight on day 4 and euthanized 12 hr later on day 4.5 post-injury. EdU was detected using Click-iT EdU Alexa Fluor 488 Imaging Kit (ThermoFisher Scientific, C10337) followed by staining with anti-MyoD antibody, Alexa Fluor 594 donkey anti-rabbit IgG antibody and DAPI[2]. Fluorescence images were captured using Metamorph Basic software (Molecular Devices) and an ORCA-flash4.0LT camera (Hamamatsu) attached to an IX73 microscope (Olympus) with a 20X LUCPlan FL N lens. Images were processed with Photoshop and Illustrator CS6 (Adobe). The minimal Feret's diameter of each

myofiber was quantified with Fiji (NIH).

Preparation of Primary Myoblasts

Mouse muscle mononuclear cells were prepared from hind limbs of 8-10 weeks old male mice as previously described[3, 4]. More specifically, muscles were minced and digested with 0.2% collagenase type 2 (Worthington, CLS-2) in DMEM to dissociate muscle cells. Satellite cells were purified with LD columns (Miltenyi Biotec, 130-042-901) by negative selection with antibodies against CD31-PE, CD45-PE, and Sca1-PE, followed by anti-PE MicroBeads (Miltenyi Biotec, 130-048-801). Positive selection was subsequently applied with an antibody against biotin-conjugated integrin α7-biotin and anti-biotin MicroBeads (Miltenyi Biotec, 130-090-485), followed by MS columns (Miltenyi Biotec, 130-042-201). Isolated satellite cells were cultured on dishes coated with 0.01% rat tail collagen (BD Biosciences, 354236) in myoblast growth medium (HAM's F-10 medium with 20% FBS, 10 ng/ml basic fibroblast growth factor (Thermo Fisher Scientific, PHG0263), penicillin (100 U/ml), and streptomycin (100 mg/ml)) at 37°C with 5% CO_2. Low-passage satellite cell-derived primary myoblasts (typically less than eight passages) were used for differentiation and immunostaining. DMEM with 5% HS, penicillin, and streptomycin was used for myogenic differentiation.

Immunofluorescence Staining of Cells

Primary myoblasts were fixed with 2% paraformaldehyde for 10 min and blocked with 1% BSA in PBS for 30 min. Permeabilized cells were stained with antibodies against MHC and MyoD and then incubated with secondary antibody Alexa Fluor 488 anti-mouse IgG and Alexa Fluor 594 anti-rabbit IgG. DNA was counterstained with DAPI. To measure proliferating primary myoblasts,

cells were pulsed with 1 μg/ml of EdU 3 hr before harvest. EdU was detected using a Click-iT EdU Alexa Fluor 488 Imaging Kit (ThermoFisher Scientific, C10337) followed by anti-MyoD antibody, Alexa Fluor 594 donkey anti-rabbit IgG antibody, and DAPI[2]. Fluorescence images were captured using Metamorph Basic software (Molecular Devices) with LUCPlanFLN 20x or 10x objective lens (Olympus) with 0.45 Ph1 aperture and a C11440-42U digital camera (Hamamatsu) attached to an IX73P2F microscope (Olympus). The images were processed with Adobe Photoshop and Illustrator CS6.

C2C12 cells were similarly stained with primary antibody against MHC, secondary antibody Alexa Fluor 488 anti-mouse IgG, and 5 μg/ml Hoechst 33342 (MilliporeSigma, B2261). Differentiation index was defined as a percentage of nuclei (Hoechst-stained structure) existing within MHC(+) cells. Fusion index is a percentage of nuclei that were located in MHC(+) cells containing more than one nuclei. Data of differentiation index, fusion index, and EdU uptake were obtained from biological triplicates in each experiment.

Western Blotting

Whole-cell extracts obtained from $2x10^5$ cells with an NE-PER Nuclear and Cytoplasmic Extraction reagents (Thermo Fisher Scientific, 78833) were loaded into a 12% SDS-PAGE gel. After completion of electrophoresis, the proteins were transferred to an Immobilon P membrane (EMD Millipore, IPVH00010) at 25°C overnight. The next day, the membrane was blocked with 5% non-fat dry milk (BioRad, 180171A) in PBT (0.2% Tween 20 in PBS) for 1 hr at 25°C. Proteins were then labeled with the primary antibody of interest diluted in 5% milk in PBT at 25°C for 1 hr. After washing with PBT for 5 min three times, the membranes were incubated with secondary antibodies goat anti-rabbit IgG-HRP or goat anti-mouse IgG-HRP both diluted at 1:1000 in 5%

milk in PBT for 1 hr at 25ºC. After washing the membrane with PBT six times, the chemiluminescence signal was detected with a SuperSignal West Dura kit (Thermo Fisher Scientific, 34075) and X-ray films.

The phospho-p38 antibody was used as follows to avoid the sequestration of the antibody by casein in the milk. The membrane was blocked with 5% non-fat dry milk in TBST (50 mM Tris-HCl pH 7.5, 0.1% Tween 20) for 1 hr at 25ºC, followed by wash with TBST for 5 min three times. The p-p38 antibody was diluted in 5% BSA in TBST and three subsequent washes were done with TBST. Goat anti-rabbit IgG-HRP was diluted in 5% milk in TBST and six subsequent washes were done with TBST.

Quantitative RT-PCR (qRT-PCR)

RNA was extracted from cells using a Quick RNA Microprep (Zymo Research, R1051) or RNeasy Plus Mini (Qiagen, 74136) kit, depending on cell number. RNA quantity and purity were assessed using a NanoDrop Lite spectrophotometer (Thermo Fisher Scientific). cDNA was synthesized with ProtoScript II Reverse Transcriptase (New England Biolabs, M0368L). Quantitative PCR (qPCR) was performed with the primers listed in Supplementary Table 3 and a GoTaq qPCR Master Mix (Promega, A6002) in a Mastercycler realplex^2 thermocycler (Eppendorf). PCR conditions were as follows: initial denaturation at 95°C for 10 min, 40 cycles of 95°C for 15 sec, 30 sec at the specific annealing temperature for each set of primers, and 72°C for 30 sec, and a melting curve step to check the specificity of the reaction. mRNA expression levels were analyzed by normalizing expression values to glyceraldehyde 3-phosphate dehydrogenase (*Gapdh*) expression. Mean ± SEM of biological triplicates with technical triplicates each were calculated.

Nascent mRNA was measured with a Click-iT Nascent RNA Capture kit (Thermo Fisher

Scientific, C10365). C2C12 cells were incubated with 0.1 mM 5-ethynyl uridine (EU) for 4 hr, followed by the isolation of EU-labeled mRNAs with magnetic beads for cDNA synthesis and qPCR.

ChIP-PCR

Two million C2C12 cells were treated with 1% paraformaldehyde for 10 min and then 125 mM glycine, followed by washing with PBS twice. Chromatin was prepared by the treatment with 300 µl cell lysis buffer (50 mM HEPES pH7.8, 85 mM NaCl, 0.5% NP-40, and cOmplete Mini Protease Inhibitor Cocktail (MilliporeSigma, 11 836 153 001)) for 15 min on ice with vortexing for 15 sec every 5 min. After centrifugation at 1,500 x *g* for 5 min at 4°C, the pellet was resuspended in 50 µl nuclear lysis buffer (50 mM Tris-HCl pH 8.0, 10 mM EDTA, 1% SDS, and cOmplete protease inhibitor cocktail) and incubated for 5 min on ice. Chromatin was sheared by sonication with a Bioruptor 300 (Diagenode) with 30 cycles of 30 sec-on and 30 sec-off with the high power setting at 4°C. After centrifugation at 15,000 x*g* for 15 min at 4°C, 5 µl supernatant ($2x10^5$ cells) was saved as input and the rest was incubated with 2 µg antibody, 2 µl Dynabeads Protein G (Thermo Fisher Scientific, 10004D), and 400 µl dilution buffer (20 mM Tris-HCl pH 8.0, 150 mM NaCl, 2 mM EDTA, 1% Triton X-100, and cOmplete protease inhibitor cocktail) for 16 hr at 4°C with rotation at 20 rpm. The beads were sequentially washed with 500 µl each of dilution buffer, LiCl buffer (20 mM Tris-HCl pH 8.0, 250 mM LiCl, 2 mM EDTA, 0.1% SDS, and 1% Triton X-100) twice, and TE (10 mM Tris-HCl and 1 mM EDTA) rotating for 5 min at 4°C each. The beads were resuspended in 100 µl elution solution (0.1 M $NaHCO_3$, 1% SDS, and 200 µg/ml proteinase K) and incubated for 2 hr at 65°C with rotation to reverse crosslink. The input was also treated in the same condition. Proteinase K was inactivated by heating for 10 min at 95°C. DNA was purified

with a ChIP DNA Clean & Concentrator (Zymo Research, D5205) and applied for qPCR as described above. Results of biological triplicates with technical duplicates each were presented as ratios in comparison to input chromatin.

The ChIP-seq data GSE25308 (Pol II, H3K4me1, H3K4me3, H3K27me3, and H3K9ac), GSE37527 (H3K27ac and p300), and GSE108650 (Bmal1) were downloaded from the UCSC Mouse Genome Browser mm9. The quality of all downloaded data was evaluated using FastQC v0.11.5 (http://www.bioinformatics.babraham.ac.uk/projects/fastqc/) and adapter sequence was trimmed using Trimmomatic v0.33 (http://www.usadellab.org/cms/index.php?page=trimmomatic)[5]. The filtered high-quality reads were then mapped to a reference genome (GRCm38/mm10) using HISAT2 v2.0.2 (https://ccb.jhu.edu/software/hisat2/index.shtml)[6]. Resulting BAM files with MACS version 2 (2.2.5) were used to generate peaks[7].

3C analysis

3C was performed combining two published protocols[8, 9]. To make a BAC control library, a mouse 110 kb BAC clone encoding *Nctc1* and *Igf2* were purchased from Thermo Fisher Scientific (RPCI23.C) and the DNA was prepared with a ZR BAC DNA Miniprep kit (Zymo Research (D4048) as control. Ten micrograms of DNA was digested with BamHI for 16 hr, followed by phenol-chloroform extraction and ethanol precipitation twice. DNA fragments were ligated with T4 ligase for 16 hr at 16°C. DNA was purified with phenol-chloroform extraction and ethanol precipitation twice and used in qPCR.

C2C12 cells were treated with 1% paraformaldehyde and then with 125 mM glycine as described in the ChIP-PCR method. Ten million cells were treated with lysis buffer (10 mM Tris-

HCl pH7.5, 10 mM NaCl, and 0.2% NP-40) for 10 min on ice. After centrifugation, the pellet was washed once with the digestion buffer for BamHI and incubated in a series of buffers for 1 hr at 37°C each: BamHI buffer, BamHI buffer with 0.3% SDS, and BamHI buffer with 0.3% SDS and 2% Triton X-100. Finally, the cells were incubated with 400 units BamHI for 16 hr at 37°C with rotation. BamHI was inactivated with 1.6 % SDS and incubation at 65°C for 30 min. The cell suspension was diluted 12-fold with lysis buffer (10 mM Tris-HCl pH7.5, 10 mM NaCl, 0.2% NP-4, and 1% Triton X-100) and incubated for 1 hr at 37°C with rotation. After addition of 100 units T4 DNA ligase, the reaction mix was incubated for 4 hr at 16°C, followed by incubation for 1 hr at 25°C. Finally, the reaction mix was incubated for 16 hr at 65°C in the presence of 300 μg proteinase K, followed by phenol-chloroform extraction and ethanol precipitation twice as a 3C library.

PCR data was analyzed as detailed in reference[8]. Briefly, PCR was performed with 10 ng BAC control library and 3C library as templates using the 3C-0 kb primer in combination with each of 3C-76 kb through 3C-112 kb primers. The primer pair 3C-Clock1 and 3C-Clock2 at the *Clock* gene, which showed a consistent amplification throughout the circadian rhythms, was used as an internal control. PCR conditions were as it follows: initial denaturation at 95°C for 5 min, 35 cycles of 95°C for 30 sec, 70°C for 30 sec, and 72°C for 20 sec, and an extension at 72°C for 5 min. PCR products were resolved with a 2% agarose gel and stained with ethidium bromide. The images were captured with a Gel Logic 212 Pro system (CareStream Molecular Imaging) and the band intensity was quantified with Fiji. Biological triplicates with technical duplicates were analyzed for each group.

RNA-seq

Total RNA was prepared from KO C2C12 cells before differentiation (day 0) and day 3 and 5 during differentiation. RNA concentration and RNA Integrity Number (RIN) were measured with an Agilent BioAnalyzer 2100. Samples with RIN over 8 were used to create sequencing libraries at the University of Minnesota Genomics Center. One microgram of total RNA was used to create each sequencing library using a Truseq RNA Sample Preparation Kit (Illumina, RS-122-2001). Briefly, poly-adenylated RNA was first purified using oligo-dT-coated magnetic beads. RNA was then fragmented and reverse-transcribed into cDNA. The cDNA was further fragmented, blunt-ended, and ligated to barcoded adaptors and amplified. Final library size distribution was validated with capillary electrophoresis and quantified with a Quant-iT PicoGreen dsDNA Assay Kit (Thermo Fisher Scientific, P11496) and qPCR. Indexed libraries were pooled and size-selected to 320 bp ± 5% with a LabChip XT (PerkinElmer). Libraries were loaded onto a single-read flow cell and amplified on a cBot (Illumina) before sequencing using a NextSeq High (Illumina).

Bioinformatics Analysis

The demultiplexed FASTQ files were analyzed using a customized pipeline (gopher-pipelines; https://bitbucket.org/jgarbe/gopher-pipelines/overview) developed and maintained by the Minnesota Supercomputing Institute. Briefly, FastQC v0.11.5 (http://www.bioinformatics.babraham.ac.uk/projects/fastqc/) was used to check on the sequencing quality of the FASTQ files. Then adapters and low-quality reads were trimmed using Trimmomatic v0.33 (http://www.usadellab.org/cms/index.php?page=trimmomatic)[5]. An additional quality check with FastQC was performed on the post-trimming sequences to ensure successful adaptor and quality trimming. The remaining sequences were then aligned to the GRCm38/mm10 reference genome using HISAT2 v2.0.2 (https://ccb.jhu.edu/software/hisat2/index.shtml) and

transcript abundance was counted using subread v1.4.6 (http://subread.sourceforge.net/)[6, 10]. Differential gene expression analysis was performed in R v3.6.2 using *edgeR* package (https://bioconductor.org/packages/release/bioc/html/edgeR.html)[11]. Gene ontology analysis of differentially expressed genes was performed by functionally annotate the genes and perform an overrepresentation enrichment test using PANTHER (http://pantherdb.org/)[12]. Heat maps were generated using the log-transformed counts with *pheatmap* v1.0.12 (https://cran.r-project.org/web/packages/pheatmap/index.html) packages. Hierarchical clustering was performed using the average linkage clustering method with the correlation coefficient as a similarity metric.

Principal component analysis

The principal component analysis was performed to investigate the clustering of the datasets. The transformed and normalized gene expression values were used and principal components were computed using the prcomp() function in R v3.6.2. The first and second largest variance components in the data (PC1 and PC2) were visualized as a scatter plot using ggplot2 v3.2.1 (https://cran.r-project.org/web/packages/ggplot2/index.html).

Scattered plot

Regression analysis was used to evaluate correlations between two groups. Normalized expression values of each group were transformed with natural log for better linear fitting and plotted against each other. R-squared value was calculated and shown on each regression line. All plots were produced in R v3.6.2 with the add-on package ggplot2 v3.2.1 (https://cran.r-project.org/web/packages/ggplot2/index.html).

Statistical Analysis

On-sided Student's t-tests were used in the analysis of statistical significance of the difference in the differentiation index, the fusion index, EdU uptake, qRT-PCR, and ChIP-PCR data. The mean + or ± SEM obtained from biological triplicates with technical triplicates was shown in each graph unless stated otherwise.

Data availability

The RNA-seq data have been deposited to Gene Expression Omnibus (GEO) under the accession number of GEO: GSE150785. Previously published ChIP-seq data that were re-analyzed here are available under the accession numbers GSE25308 (Pol II, H3K4me1, H3K4me3, H3K27me3, and H3K9ac), GSE37527 (H3K27ac and p300), and GSE108650 (Bmal1). Other data that support the findings of this study are available upon reasonable request from the corresponding authors.

References

1. Shimizu-Motohashi, Y. *et al.* Pregnancy-induced amelioration of muscular dystrophy phenotype in mdx mice via muscle membrane stabilization effect of glucocorticoid. *PLoS One* **10**, e0120325 (2015).
2. Verma, M. *et al.* Muscle Satellite Cell Cross-Talk with a Vascular Niche Maintains Quiescence via VEGF and Notch Signaling. *Cell Stem Cell* **23**, 530-543 e539 (2018).
3. Asakura, A., Seale, P., Girgis-Gabardo, A. & Rudnicki, M.A. Myogenic specification of side population cells in skeletal muscle. *J Cell Biol* **159**, 123-134 (2002).
4. Motohashi, N., Asakura, Y. & Asakura, A. Isolation, culture, and transplantation of muscle satellite cells. *J Vis Exp*, doi: 10.3791/50846 (2014).

5. Bolger, A.M., Lohse, M. & Usadel, B. Trimmomatic: a flexible trimmer for Illumina sequence data. *Bioinformatics* **30**, 2114-2120 (2014).

6. Kim, D., Langmead, B. & Salzberg, S.L. HISAT: a fast spliced aligner with low memory requirements. *Nat Methods* **12**, 357-360 (2015).

7. Zhang, Y. *et al.* Model-based analysis of ChIP-Seq (MACS). *Genome Biol* **9**, R137 (2008).

8. Naumova, N., Smith, E.M., Zhan, Y. & Dekker, J. Analysis of long-range chromatin interactions using Chromosome Conformation Capture. *Methods* **58**, 192-203 (2012).

9. Hagege, H. *et al.* Quantitative analysis of chromosome conformation capture assays (3C-qPCR). *Nat Protoc* **2**, 1722-1733 (2007).

10. Liao, Y., Smyth, G.K. & Shi, W. featureCounts: an efficient general purpose program for assigning sequence reads to genomic features. *Bioinformatics* **30**, 923-930 (2014).

11. Robinson, M.D., McCarthy, D.J. & Smyth, G.K. edgeR: a Bioconductor package for differential expression analysis of digital gene expression data. *Bioinformatics* **26**, 139-140 (2010).

12. Mi, H., Muruganujan, A. & Thomas, P.D. PANTHER in 2013: modeling the evolution of gene function, and other gene attributes, in the context of phylogenetic trees. *Nucleic Acids Res* **41**, D377-386 (2013).